Encoding seizures with partial synchronization: A spiking neural network for biosignal monitoring on a mixed signal neuromorphic processor

Jim Bartels[2,1], Olympia Gallou[1,3], Hiroyuki Ito[2], Matthew Cook[1], Johannes Sarnthein[3,4], Giacomo Indiveri[1,4,*], and Saptarshi Ghosh[1]

[1]Institute of Neuroinformatics, University of Zurich and ETH Zurich, Zurich, Switzerland
[2]Nano Sensing Unit, Tokyo Institute of Technology, Yokohama, 226-8503, Japan
[3]Department of Neurosurgery, University Hospital Zurich, University of Zurich, Zurich, Switzerland
[4]Zurich Neuroscience Center, ETH Zurich and University of Zurich, Zurich, Switzerland
[*]giacomo@ini.uzh.ch

ABSTRACT

Long-term monitoring of biomedical signals is crucial for modern clinical treatment of neurological disorders such as epilepsy. Encoding epileptic seizures with partial synchronization using a spiking neural network (SNN) offers a promising avenue as such networks can be implemented on ultra-low-power neuromorphic processors. Indeed, such bio-inspired neuromorphic systems containing mixed-signal asynchronous electronic circuits can perform always-on monitoring of biomedical signals for extended periods of time, without having to employ traditional clocked analog-to-digital conversion or cloud-based processing platforms.

Here, we present a novel SNN architecture, co-designed and implemented with a mixed-signal neuromorphic chip, for monitoring epileptic seizures. Our hardware-aware SNN captures the phenomenon of partial synchronization within brain activity during seizures. We validate the network on a full-custom mixed-signal neuromorphic hardware using real-time analog signals converted from an Electroencephalographic (EEG) seizure data-set, and encoded as streams of events by an asynchronous delta modulation (ADM) circuit, directly integrated, together with its analog front-end (AFE) signal conditioning circuits, on the same die of the neuromorphic SNN chip.

We demonstrate the ability of the hardware SNN to extract local synchronization patterns from the event streams and show that such patterns can facilitate seizure detection using a simple linear classifier. This research represents a significant advancement toward developing embedded intelligent "wear and forget" units for resource-constrained environments. These units could autonomously detect and log relevant EEG events of interest in out-of-hospital environments, offering new possibilities for patient care and management of neurological disorders.

1 Introduction

Studies on the dynamics and modeling of the brain with non-linear systems have led to valuable insights into its behavior[1]. One particular aspect of such association involves the emergence of synchronous patterns in neural activities[2] and their use in explaining neural disorders, including epileptic seizures[3,4]. Epilepsy is one of the most common neurological disorders in the world, affecting nearly 1% of all people worldwide in all age groups[5,6]. It is primarily characterized by chronic seizures which are a localized, highly synchronous brain activity characterized by high amplitude neural signals that can be captured by Electroencephalographic (EEG) recordings in the clinical setting at a high level of confidence[7]. Seizure detection in the EEG is a wide field of scientific interest that relies on current advances in biomedical sensing, intelligent Application Specific Integrated Circuits (ASICs), and advanced machine learning algorithms[8–11]. The EEG dynamics during seizures have recently been associated with a special partially synchronous state, termed "chimera", where temporarily correlated, synchronous, and non-synchronous groups spontaneously emerge[12,13]. Such states can provide valuable information in both understanding the disorder as well as help in its monitoring.

A common approach to seizure monitoring currently utilizes a combination of limited in-person clinical observation and outside the clinical setting, a patient-maintained log known as a "seizure diary" (Fig. 1a), which however suffers from over- and underreporting[14]. To improve on seizure monitoring, several devices for automated seizure detection have been validated[15]. These devices record a selection of various biosignals, among them EEG, electrocardiogram, electromyography, electrodermal activity, and accelerometry where EEG remains the most reliable. Two pioneering

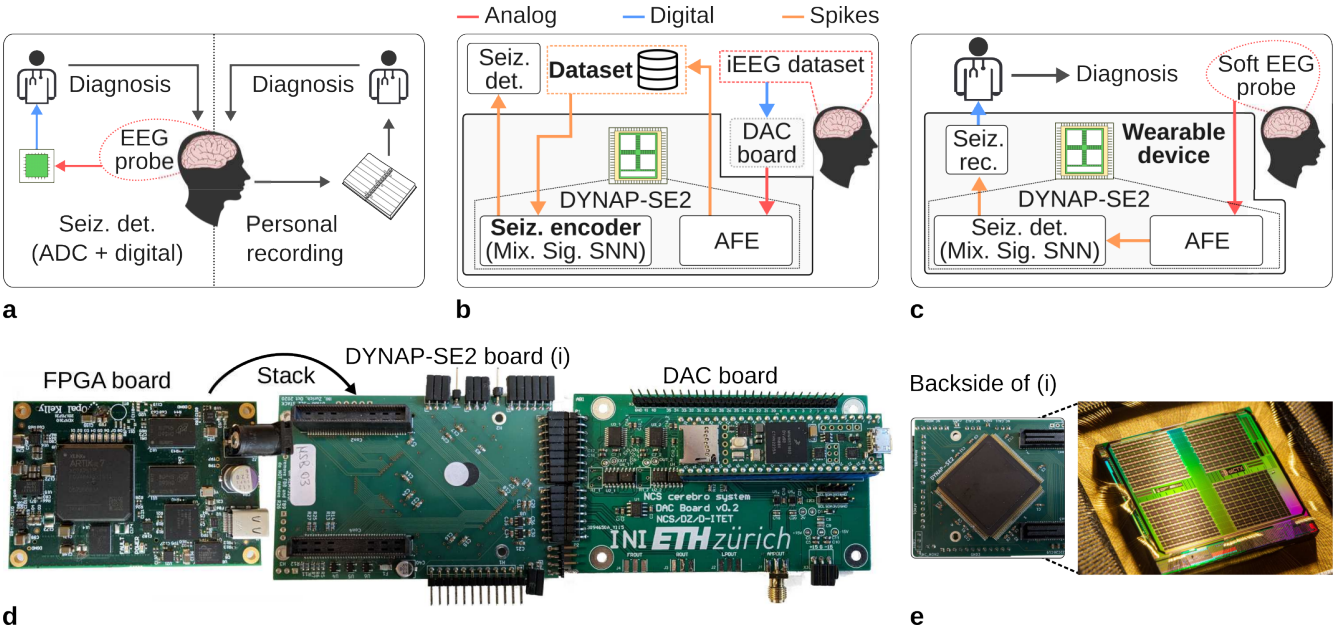

Figure 1. Overview of existing, presented, and proposed seizure detection systems, and a diagram of the setup constructed for this work; **a** SOA (state of art) approaches for seizure detection and diagnosis; seizure recording with a seizure diary (right side), seizure detection using Analog-to-Digital Converters (ADC) and digital processing (left side); **b** Presented system; seizure encoding on DYNAP-SE2 with analog iEEG signals using on-chip Analog Front-End (AFE) and a Spiking Neural Network (SNN); **c** Envisioned system; real-time seizure detection pipeline with DYNAP-SE2 and a seizure recorder within a wearable device; **d** Photographs of the setup, an FPGA board, DYNAP-SE2 board with DYNAP-SE2 chip on the underside, Digital-to-Analog (DAC) converter board with a Teensy microcontroller for interfacing with the AFE; **e** Photograph of the DYNAP-SE2 die (right), and the package located on the underside of the DYNAP-SE2 board (left).

devices in the domain of classical EEG-based monitoring field are the seizure advisory system (SAS) developed by NeuroVista Corporation[16] and the responsive neurostimulation system (RNS) of Neuropace Corporation[17]. Although promising, both of these digital devices show the same constraints in long-term beyond-laboratory monitoring, namely, resource-intensive operation and inefficient A/D conversion with power-limited system clock. Thus, on a system level, these setups may consume a substantial portion of the overall power, limiting their use for long-term monitoring.

The neuromorphic engineering research field, which is inspired by the principles of computation of biological neural systems[18,19], represents a promising approach for implementing low-power always-on electronic processing systems applied to biomedical signal processing[20]. Neuromorphic computing has enabled the development of extremely efficient architectures[21] that are built with synapse and neuron circuits, arranged in a highly parallelized fashion and operating asynchronously[22]. As a result, various neuromorphic devices have emerged, ranging from *LoiHi* and *SpiNNaker*, where neurons are simulated digitally using numerical integration of neuron equations[23,24], to *BrainScaleS* and *DYNAP-SE* where neural primitives are implemented in custom analog circuits, connected by a digital event-routing fabric[25,26].

In this work, we present a novel on-chip two-layered Spiking Neural Network (SNN), compatible with mixed-signal analog/digital neuromorphic hardware, that encodes the partial synchronization of brain states during seizure (ictal) periods by means of firing rate-based filtering and a specific connectivity structure. We validate the model on a full-custom hardware pipeline that does not require any digital compute element in the loop. The model network was implemented in neuromorphic hardware using the spiking neuron circuits of the DYnamic Neuromorphic Asynchronous Processor (DYNAP-SE2)[27], as shown in Fig. 1e.

To convert the EEG signals into streams of spikes that can be sent in as input to the SNN, we used an Analog Front End (AFE) circuit containing low-noise amplifiers, filters, and an Asynchronous Delta Modulator (ADM) circuit[28] directly integrated in the DYNAP-SE2 chip. As a major advance over previously reported related approaches[29,30], signal conditioning, spike encoding, and SNN processing are all realized on the same chip. Utilizing an input AFE,

ADM, and a recording setup (Fig. 1d), we created an event-based intracranially recorded iEEG dataset from the SWEC-ETHZ iEEG Database[31]. By combining signal conversion and processing stages on the same chip, we built an integrated proof-of-concept setup for encoding seizures with network synchronization properties (Figs. 1b and d).

Rather than following the classical Machine learning (ML) approach of training artificial neural networks (ANNs) with large data-sets, our proposed SNN that is at the same time biologically inspired and (as a consequence) compatible with neuromorphic hardware, amplifies and extracts the intrinsic partial synchronization (i.e., "Chimera") patterns that are present (but not prominent) in the input signals. By designing a hardware-compatible shallow spiking neural network that couples the encoded input spike-trains in an adjacent but non-global fashion, the neuromorphic processing system developed is able to mimic correlation and form synchronized clusters. This mechanism is indicative of the network's ability to mirror partial synchronous states observed in the EEG recordings during seizures, representing the first proof-of-concept for encoding seizures through partial synchronization in real-time neuromorphic hardware.

The hardware implementation of this SNN, on the DYNAP-SE2 chip, is able to produce the desired results because it exploits the rich dynamics arising from sub-threshold analog circuits, as well as the heterogeneity present in its synapses and neurons due to device mismatch effects. We show how this mixed-signal hardware setup preserves all of the information present in the original data, by comparing the classification accuracy on the spiking data with that of a Support Vector Machine (SVM) on the original input data. To our knowledge, no prior work exists that encodes in real-time such states with a network on a neuromorphic device to provide seizure indications.

The main contribution of the work described in this article is the development of a foundational network dynamics-based approach for biomedical signal monitoring using mixed-signal neuronal circuits. The possibility of long-term processing of the data obtained using this approach, combined with its robust signal processing features, will further allow the development of wearable epileptic seizure detection and logging systems in the future (Fig. 1c). The general framework of analyzing and processing long-term recordings to detect and possibly predict events of interest has the potential to be useful also for a wide range of different applications, both in the healthcare and medical domain (e.g., for cardiovascular or diabetic diseases) and in other "edge computing" domains.

2 Results

2.1 Asynchronous Delta Modulation (ADM) of EEG signals

The first stage of the processing pipeline is outlined in Fig. 1b. It comprises the AFE and ADM blocks embedded in the DYNAP-SE2, for encoding analog EEG signals into events. Figure 2 shows recorded analog waveforms from two EEG input channels (Channel 12 and 13 of a single seizure of patient 1), selected from the SWEC dataset[31]. Figure 2a presents the oscilloscope traces of the analog EEG signal. These traces were obtained by converting the digitized dataset waveforms back into analog signals using a DAC setup (Fig. 1b, left) and amplified by the initial stage of the AFE. The amplified signal stream of the AFE is then inputted to the ADM, which produces asynchronous streams of Up and Down pulses, depending on the slope of the analog waveform (See Methods section). The Up and Down events are shown above and below the analog waveforms and the event rate is color-coded as per the colorbar (Fig. 2 right). A close-up of 16 seconds of the first channel (zoomed plot above Fig. 2b) shows the increase of event rates and their burstiness during the seizure (ictal) periods. The conversions with the AFE are recorded in an "event-based hardware encoded dataset" (see data availability). In total, we encoded and made publicly available[32] data for ten seizures, two per patient for a total of five patients. The events from the ADM circuits are fed as single pulse trains per channel into the SNN core of the DYNAP-SE2.

2.2 The DYNAP-SE2 SNN implementation: firing-rate filtering and encoding correlation

The second stage of the pipeline outlined in Fig. 1b is the SNN model implemented on the DYNAP-SE2. Figure 3a shows the SNN architecture. It comprises two layers: a "translation" layer and a "non-local non-global" (NLNG) encoding layer. The translation layer, adapted from Sava et al.[33], consists of Recurrent Excitatory (R-E) and Inhibitory (R-I) neurons, combined with a Feed-Forward Inhibitory neuron (FF-I) depicted in Fig. 3a (left). The FF-I and the R-E neurons receive events from the AFE-converted event streams for iEEG signal channels via a slow-excitatory synapse. Further, the R-E neurons are inhibited by the output spikes from FF-I neurons via a slow-inhibitory synapse. The R-E and R-I neurons represent a neuron pair that both excite and inhibit each other, constructing an excitatory-inhibitory (E-I) balance pair.

Figure 3b shows the firing rate input-output curve of the translation layer in the DYNAP-SE2 based on input Poisson trains of varying firing rates. The synaptic time constants of all neuron types (R-E, R-I, and FF-I) have been set heuristically to achieve the frequency transfer curve in Fig. 3b. All other parameters including the weights were

left constant (see Methods for parametric values). The FF-I neurons have a high synaptic time constant, leading to a firing rate that saturates at around 180 Hz for input firing rates $>$200 Hz. These neurons inhibit low-frequency input spikes (Fig. 3c). The slow inhibition of the R-E neurons by R-I neurons results in a near-linear output firing rate between 200 Hz to 600 Hz (Fig. 3d). The above represents a spike-based non-linear filter, i.e., the excitation of the R-E, -I neurons is highly sensitive to the 200–600 Hz firing rate band while insensitive to inputs from outside this band.

The second layer, termed the NLNG encoding layer, is excited by the R-E neurons of the translation layer with a specific connectivity structure. The connections consist of slow excitatory synapses with constant synaptic weights. The constant weight per synapse is chosen to make sure that the membrane potential of the neurons reaches close to the set threshold. The connectivity structure is described by a 1 – 2 – 1 – 0 – 1 – 2 – 1 connectivity between the R-E and NLNG neurons (Fig. 3a) where 2 represents a synapse with a weight twice the constant weight mentioned above (see Methods for parametric values). To give an example, we consider 42 input neurons (encoding the 42 EEG channels, for the case of a particular patient), producing 42 outputs from R-E neurons as per the frequency response curve shown in Fig. 3b. Here, the R-E neuron from a translation block n is connected to the neighboring NLNG neurons (n-3,n-2,n-1 and n+1,n+2,n+3, mirrored) with one synapse, two synapses with constant weight (representing one synapse with 2$\times$ constant weight), and one synapse, respectively. This connectivity pattern is mirrored on both sides while ignoring NLNG neuron n itself. The connectivity structure is shown in Fig. 3a and is similar to a regular graph[34]. Such connectivity patterns are established for each R-E neuron connected to the NLNG layer with closed boundary conditions.

This connectivity matrix between these layers is determined by a neural architecture search using a *differential evolutionary* algorithm with a cost function defined as the maximum separation between output firing rate from non-correlated input and correlated Poisson input.

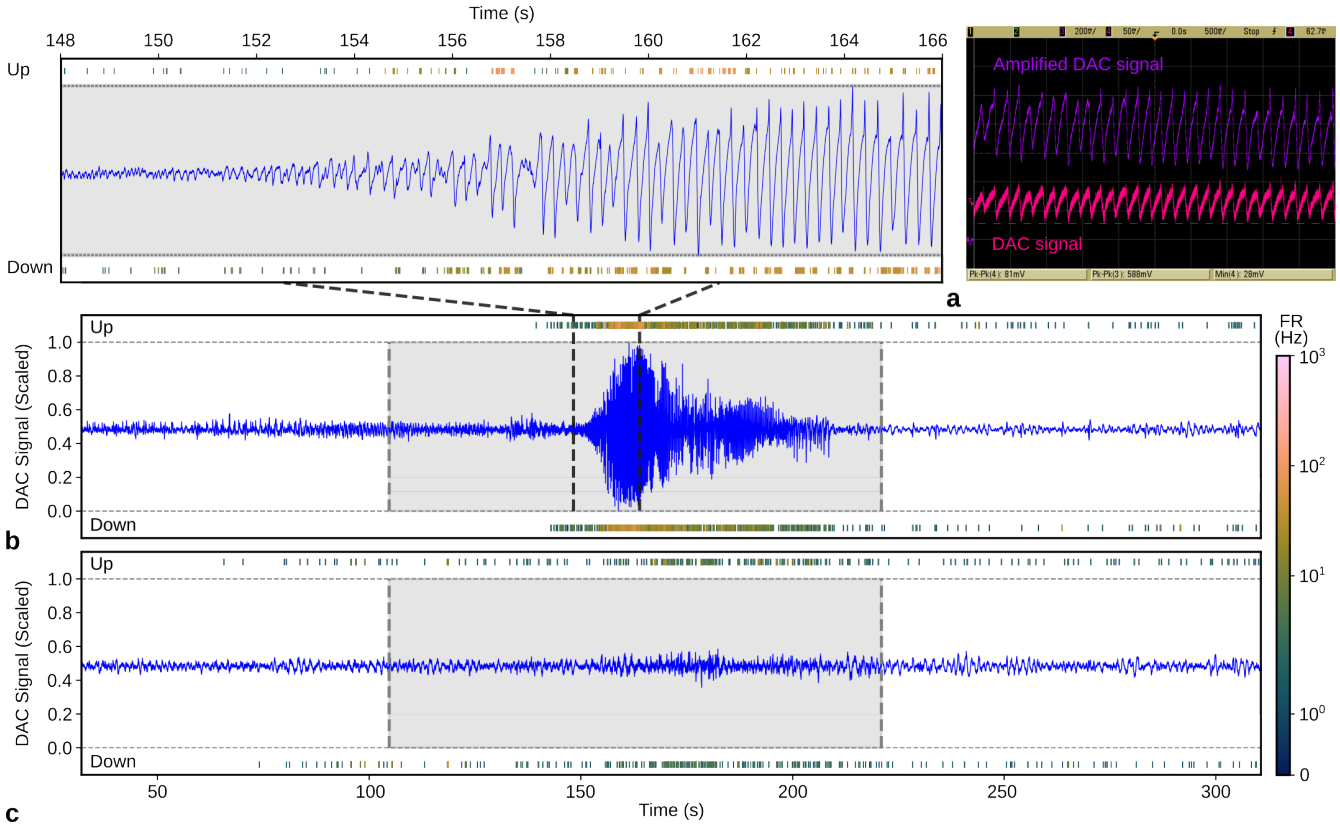

Figure 2. Snippets presenting 320-second long DAC converted analog iEEG signals from two channels and the encoded events from the ADM ('*UP*' and '*DOWN*') on DYNAP-SE2. The event rate (above and below the DAC-generated signal) is encoded in color with the seizure period denoted by the grey background; **a** Oscilloscope traces depicting the incoming DAC-generated signal (trace 4, in pink) and the AFE amplified signal (trace 3, in purple); **b** Analog waveform of one EEG channel and ADM events (with inset above showing a close-up of 16 seconds); **c** Analog waveform of another EEG channel and ADM events.

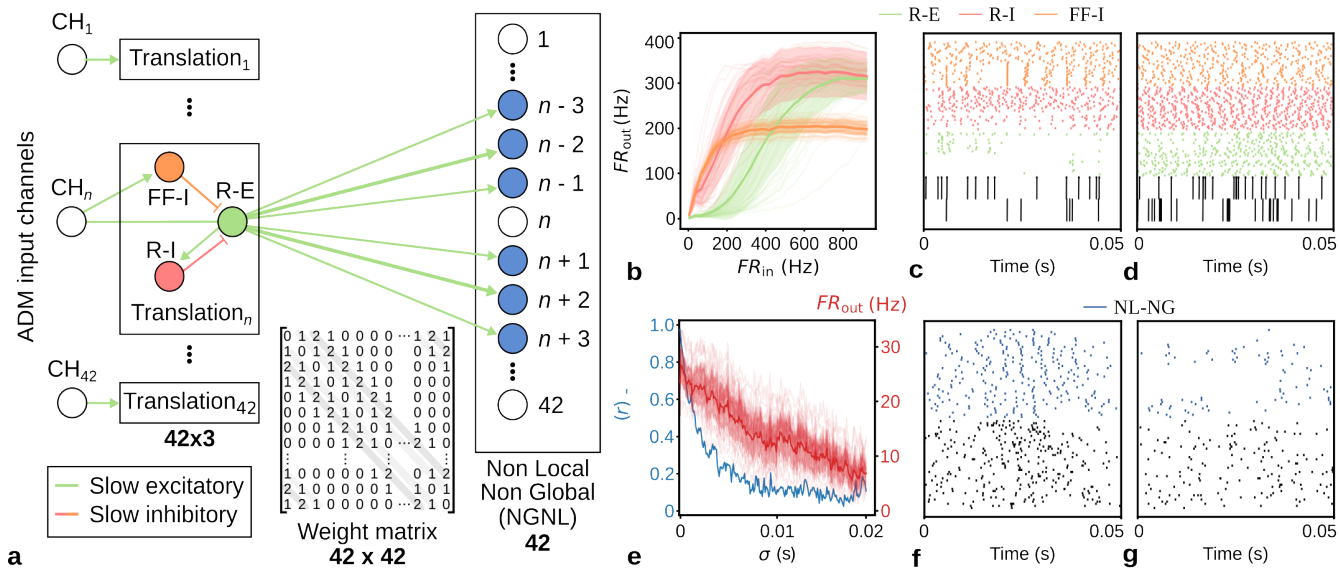

Figure 3. a Structure of the on-chip SNN; a translation layer containing 3 types of neurons, Feedforward Inhibitory (FF-I), Recurrent-Excitatory (R-E), and Recurrent Inhibitory (R-I) neurons. This layer performs firing-rate-based filtering, followed by a Non-Local Non-Global (NLNG) layer. Synapse types slow excitatory (NMDA like) and slow inhibitory (GABA-B like) are color-coded; **b** Firing rate input-output curve as a result of Poisson-generated input spikes to translation layer; **c**, **d** Raster plots of the translation layer for an input firing rate of 200 Hz and 400 Hz respectively; **e** In blue, the mean Pearson correlation coefficient of 42 input channels over the standard deviation of jittering in spike time at input firing rates of 50 Hz. In red, the output firing rate of the non-local non-global encoder as a result of the jittered input spike trains; **f**, **g** Raster plots of input (black) and output of the non-local non-global encoder (blue) at standard deviations of $\sigma = 0.005$ s and $\sigma = 0.015$ s.

Figure 3e shows a linearly inverse relationship in the output firing rate of the NLNG layer from DYNAP-SE2 with the correlation between input spike-trains. These spike trains are generated from a Poisson process and iteratively jittered with jitter noise taken from a normal distribution and input simultaneously across 42 channels to the chip. The NGNL layer exhibits a firing rate near 25 Hz for fully correlated input spike trains, decreasing to 20 Hz and 10 Hz for less correlated spike trains, with mean Pearson correlation coefficient of r =0.255 and $r = 0.114$, arising from spike time jitter noise at standard deviations of $\sigma = 0.005$ s and $\sigma = 0.015$ s respectively (Fig. 3f and g). This experiment shows the functionality of this layer and its ability to encode correlation between input channels by means of firing rate for ideal Poisson inputs.

2.3 Encoding seizures with partial synchronization using the hardware SNN

The above presented network is used for a proof-of-concept of real-time on-chip seizure encoding using the event-encoded EEG signals described in the previously mentioned ADM section. As the dynamics of these events are substantially distinct from Poisson-based spike trains (Fig. 2b), we reduced the time-constant of the NLNG neurons compared to the previous section. We further analyzed the output of the NLNG neurons by means of synchronization matrices.

Figure 4a shows 42 raw iEEG waveforms of the first seizure of patient 1 from the SWEC-ETHZ dataset with annotated ictal (seizure) period (indicated by the grey area). The events of each EEG channel are simultaneously fed to the SNN cores of DYNAP-SE2 in real-time (Fig. 4b, row-1). The translation layer rejects the lowest firing rate input spikes and reduces high input firing rates (Fig. 4b, rows 2,3,4) while keeping a linear relationship between the input and output firing rates in intermediate areas similar to Fig. 3b.

The NLNG layer shows a high firing rate for the R-E neuron inputs that is correlated locally, best observed between t = 125 s and t = 190 s in Fig. 4b. Furthermore, a firing rate nearing 50 Hz can be observed in the pre-seizure period, between t = 0 s and t = 40 s across R-E neurons 15 to 30. Here, the NLNG layer does not spike at firing rates >100 Hz. Moreover, during the period of time t > 40 s, most of the firing rate from this group of R-E neurons disappears. Adversely to this reduction, the firing rate of neurons 20 to 25 in the NLNG layer increases substantially to values above 100 Hz and continues to increase until the seizure ends. This points towards the

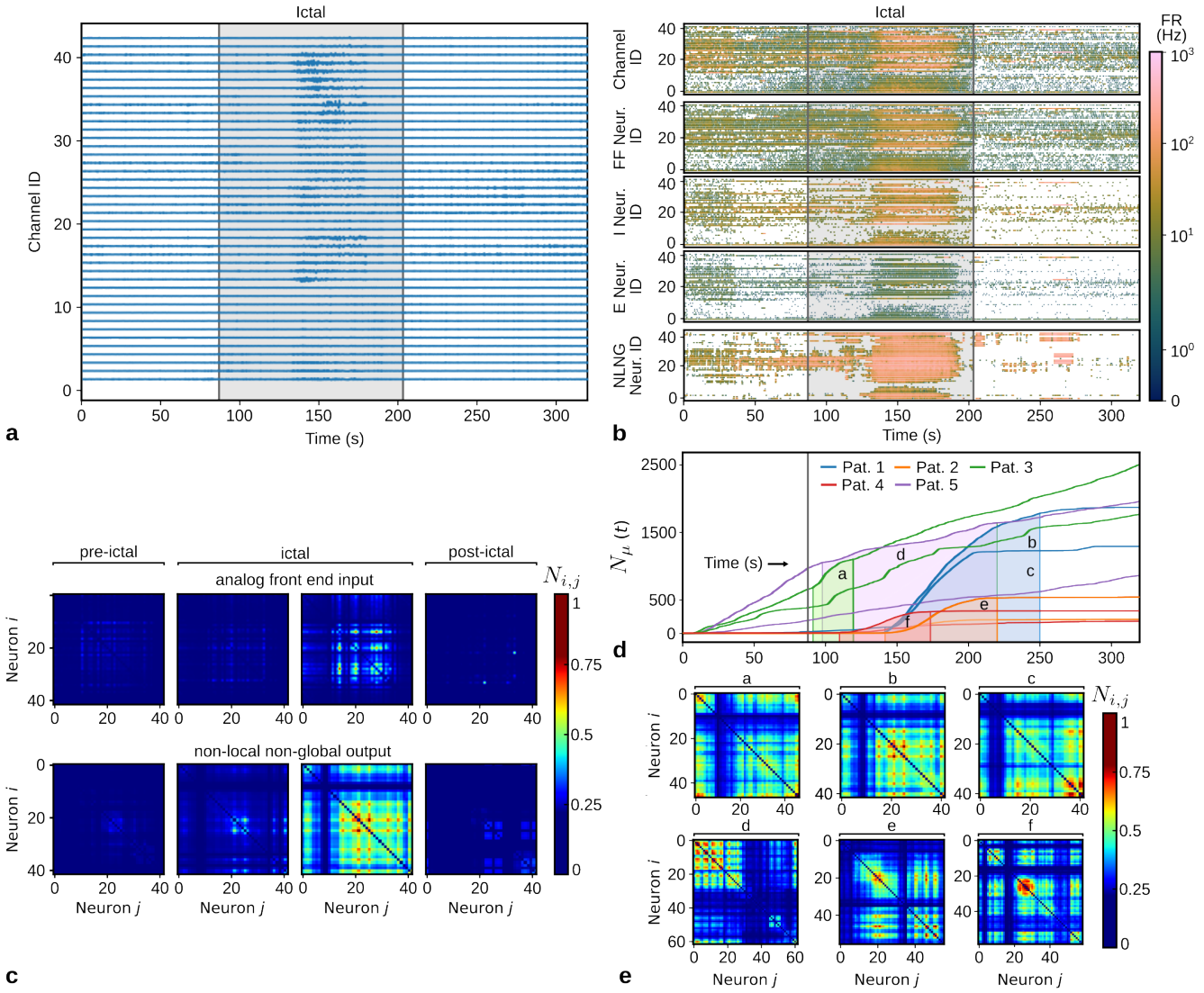

Figure 4. **a** 42 channels of input EEG signals from patient 1, seizure 1; **b** Output rasterplots of the DYNAP-SE2 on-chip implemented network. Top row to bottom: ADM-encoded input of **a**, Feedforward (FF) inhibitory neurons' outputs, Inhibitory (R-I) and Excitatory (R-E) neurons' outputs of the E-I pairs, and outputs of the Non-Local-Non-Global (NLNG) neurons. The firing rate is color-encoded per one-second time-segment; **c** Normalized synchronization matrices between channel and neuron pairs of AFE input and NLNG output, respectively. From left to right: the pre-ictal, ictal, and post-ictal periods. The synchronization matrices during the ictal period (2nd and 3rd column) are created from the first half and second half of the seizure in time, respectively; **d** The mean synchronization over all pairs of the NLNG layer cumulatively summed over time, colored areas under the curve indicate a hand-selected period of time used to construct synchronization matrices in **e**; **e** Synchronization matrices taken during periods of maximal synchronization.

dominant excitation of the NLNG layer, namely correlated input even at low firing rates.

In addition to the above analysis, we have employed kernelized spike trains with causal exponentially decaying functions[35], denoted as $f_i(t)$ where i indicates the NLNG neuron index. Using these kernelized spike-trains, we determine a measure of synchronization by taking the Manhattan (L_1) norm of the inner product between neuron pairs i and j, $N_{i,j} = || < f_i, f_j > ||_1$ and average them over a fixed time period; see Methods for a step by step explanation. In essence, we define synchronization as the similarity of spike-trains between neurons over fixed time periods and quantify it with the above.

Figure 4c shows the normalized synchronization matrices between each AFE event stream (top) and each

NLNG neuron $N_{i,j}$ pair (bottom) for a single seizure. These matrices demonstrate the functionality of the NLNG layer, namely, the enhancement of the inherent correlation structure present when seizures occur. Fig. 4d shows the accumulated Manhattan norm over time which confirms that these emergent synchronization phenomena are replicated by the NLNG layer across all patients during the seizure period. The clusters emerging in Fig. 4e for different patients in the seizure period (as labeled in Fig. 4d) show emergent localized synchronization.

Patient	Specificity [%] AFE / NLNG	Sensitivity [%] AFE / NLNG	Accuracy [%] AFE / NLNG
1	96.0 / 92.2	90.3 / 91.5	92.9 / 91.8
2	95.4 / 94.5	80.3 / 83.0	89.3 / 89.8
3	76.3 / 70.4	87.3 / 90.2	82.8 / 82.3
4	97.0 / 93.1	77.9 / 76.8	91.7 / 88.6
5	85.6 / 83.2	79.9 / 79.4	83.1 / 81.4

Table 1. Seizure classification results and Engel scores with a linear SVM that uses the Analog Front End (AFE) and encoded features of the Non-Local Non-Global (NLNG) layer as input.

2.4 Detecting seizures using SNN encoded features

The output spike trains of the NLNG layer and the original AFE input are used as features for seizure detection with a linear classifier offline. This empirically shows the ability of the SNN on DYNAP-SE2 to distinguish between ictal and non-ictal periods. In this case, our proposed SNN on DYNAP-SE2 described in Fig. 3 functions as a feature encoder, mapping raw input data onto a hyperdimensional plane that can subsequently be read out and decoded. The output spike trains of the NLNG layer are publicly available (see data availability statement) to allow for any follow-up studies without requiring access to a DYNAP-SE2. For the sake of brevity, we show the separability of ictal and non-ictal periods by employing a linear Support Vector Machine (SVM) and firing-rate binning.

The NLNG and AFE spike trains are binned with one-second windows, channel by channel, normalized, and used to classify ictal and non-ictal periods using a linear SVM. Bayesian optimization and 5-fold cross-validation with stratified splitting are employed for training and testing. Table 1 describes the result of seizure detection per patient. We are able to achieve accuracy between 81.4–91.8% with a specificity and sensitivity of 70.4–94.5% and 76.8–91.5% respectively using the NLNG layer. These performance metrics are similar to the AFE input with an accuracy between 83.1–92.9% and a specificity and sensitivity between 76.3–97.0% and 77.9–90.3% respectively.

3 Discussion

This work presents a neuromorphic approach towards a real-time seizure monitoring system by employing asynchronous delta modulation based encoding and analog neuronal dynamics on-chip. Instead of the conventional machine learning training methods for solving bio-signal processing tasks with digital computing systems, the approach proposed capitalizes on the inherent dynamics of analog neurons embedded within the hardware. Moreover, compared to conventional seizure-detection systems[15], the prototype embedded system developed does not operate based on a global system clock but processes signals in a real-time data-driven mode with asynchronous encoding, spike routing, and analog neurons[27]. This is a distinct advantage in terms of power consumption and scalability for always-on applications as for most of its operational time, in the absence of high energy inputs, the system is silent, significantly prolonging the monitoring period[36,37].

The observation that the NLNG layer imitates the ictal state in real-time by forming partially synchronized clusters within itself can be studied to understand the temporal characteristics of seizure patterns. Future work could involve investigating the formation of the synchronized clusters through time and mapping their relation to the location of the recording channels, helping in tracking the progression of the seizure. Such work can help in the identification of the seizure onset zones that are responsible for seizure generation and provide insights into the disorder itself.

Classification with a linear SVM shows that the NLNG neurons are capable of separating ictal and non-ictal periods. However, we note that the accuracy of such an offline linear classifier does not change much between the firing rate of AFE-encoded event streams and NLNG-encoded spike streams, which shows that the firing rate in the current setup is not a good feature for seizure detection. On the other hand, the correlation patterns between

neuron pairs in the AFE event streams and the NLNG spike streams vary significantly (Fig. 4c). This suggests a future investigation avenue to design an event-based output layer that can perform seizure detection based on the correlation patterns of neuron pairs taking advantage of the emergent locally synchronized clusters. This approach can also be expanded for the identification of different temporal zones in a seizure event and also might help with the classification of seizure types based on partially-synchronized cluster patterns. However, we note that the currently utilized linear SVM is limited due to the use of firing-rate encoded features from the NLNG layer. Further work is necessary to determine on-chip neuromorphic approaches for implementing the decoding of the NLNG layer into different classes dealing with either seizure types or the characterization of temporal domains.

This work serves as a gateway to a more universal approach to exploiting the dynamics of analog neurons and their use in classification tasks. The NLNG layer, coupled with event-encoded input channels through a tuned translation layer, showcases the potential of analog computation in encoding the non-linear dynamics of a complex system. As is exemplified by the structure of the NLNG weight matrix, we believe network structure, emphasizing topology and reciprocity, appears particularly well-suited to the intricacies of mismatched neuromorphic devices. Given the inherent variability of on-chip weights and parameters in mixed-signal or analog neuromorphic devices[38], integrating the lottery ticket hypothesis[39,40] with the hardware's dynamical and topological properties could pave the way for additional advancements. We believe this interdisciplinary approach could open up new avenues for the widescale adoption of these devices in a diverse number of applications that are not limited only to bio-medical domains but expand into any complex systems.

4 Conclusions

This article presents a first step towards a real-time event-based seizure monitoring system. We introduced an event-based EEG seizure dataset created with an on-chip AFE followed by an SNN with special connectivity to encode seizures with a mixed-signal neuromorphic device. The SNN on-chip shows a proof-of-concept to encode seizures during ictal periods using its inherent dynamical properties.

To our knowledge, this is the first human EEG seizure dataset that has been encoded into events using a real-time delta-modulator. The dataset and synchronization encoded spike trains have been made publicly available[32]. The framework of this investigation provides, on the one hand, the detailed specifications for the design of new front-ends and SNNs implemented on neuromorphic hardware, optimized for on-edge seizure monitoring, and on the other creates a foundation for the design of a more general class of always-on embedded and low-power neural network computing systems for a wide range of biomedical signal processing tasks.

5 Methods

The DYNAP-SE2 neuromorphic processor contains analog exponential integrate and fire (Exp I&F) neuronal and synaptic circuits with spike-frequency adaptation. The DYNAP-SE2 also hosts the AFE including the level-crossing Asynchronous Delta Modulator (ADM) circuit on the same die. Here, we describe the equations of the Exp I&F neurons and synapses derived from the circuit equations of DYNAP-SE2. This is followed by an explanation of the AFE and a description of the neuron cores of DYNAP-SE2. Afterward, we introduce the approach to compute the correlation and construct the synchronization matrices, followed by a detailed event-based dataset description.

5.1 Neuron and synapse models

The neurons of the SNN in this work consist of current-mode Exp I&F neuron circuits. The detailed description of the circuit equations in the sub-threshold regime and their deduction leading to this simple form is described by Chicca et al.[19]. Omitting the adaptation term, this equation is shown by

$$\tau(1+\frac{I_{th}}{I_{mem}})\frac{d}{dt}I_{mem}+I_{mem}=\frac{I_{th}}{I_{\tau}}(I_{in}-I_{\tau})+f(I_{mem}) \tag{1}$$

where I_{mem} is the subthreshold current depicting the membrane potential of the silicon neuron. Other terms including the time constant and the threshold can be defined as follows:

$$\begin{aligned} \tau &\triangleq \frac{C_{mem}U_T}{\kappa I_{\tau}} \\ I_{\tau} &\triangleq I_0 \exp\frac{\kappa}{U_T}v_{lk} \\ I_{th} &\triangleq I_0 \exp\frac{\kappa}{U_T}v_{thr} \end{aligned} \tag{2}$$

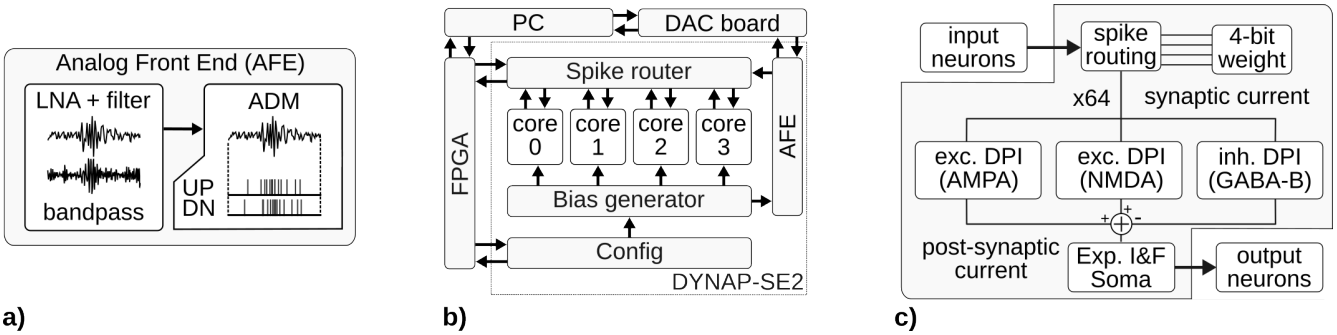

Figure 5. a Internal components of the Analog Front End (AFE), a Low-Noise Amplifier (LNA) with bandpass filter followed by the Asynchronous Delta Modulator (ADM); **b** Block diagram of the boards and DYNAP-SE2: the FPGA sends input spikes to the spike cores and configures the AFE and SNN cores; a DAC board interfaces directly with the AFE; **c** Neuron schematic. Input events are translated to synaptic currents. The synaptic currents are routed to one of four synapse types, each combined with Differential Pair Integrators, and forwarded to an Adaptive Exponential Leaky Integrate & Fire soma.

U_T is the thermal voltage, κ is the subthreshold slope factor stemming from the capacitive coupling ratio from gate to channel and I_0 is the transistor dark current which are constants of the n-type MOSFETs used in the circuit[41]. The non-linear term comes from $f(I_{mem})$ which has been experimentally shown to be an exponential function of I_{mem}[42].

The synapses of the DYNAP-SE2 are modeled after the DPI circuit[43] and can be represented in a simplified form as

$$\tau \frac{d}{dt} I_{out} + I_{out} = I_{in} \frac{I_w}{I_\tau} \tag{3}$$

where I_{out} is the output current, the time constant is $\tau \triangleq \frac{C_{syn} U_T}{\kappa I_\tau}$, where I_τ is a bias current, and $I_{in} \triangleq I_0 \exp \frac{\kappa}{U_T} v_{in}$ is the input current.

5.2 AFE and encoding setup

The dataset chosen in this work consisted of intracranially recorded iEEG signals which after undergoing 16-bit analog-to-digital conversion, and being band-pass filtered between 0.5 and 150 Hz, were recorded digitally at a sampling rate of 512 Hz. To mimic a real-world scenario, we utilized a DAC stage (acting as a virtual sensor) to convert the digitally recorded waveforms of the dataset into analog signals. This DAC stage consists of an 18-bit DAC (AD5781, Analog Devices, Wilmington, MA) and a custom PCB (designed with support from the Microelectronics Design Center of ETH Zurich), allowing regeneration of the digital data into corresponding analog waveforms (Fig. 1d). The DAC is controlled by a microcontroller (Teensy 4.1 from PJRC, Sherwood, OR) which transmits a digital signal stored in an SD card to the DAC via an SPI bus. The input signal is generated with a ∼100 mV peak-to-peak voltage and with a ∼30 mV offset for all DAC conversions. The EEG signal amplitude is scaled to such values considering the DAC PCB and AFE characteristics. A sample from the oscilloscope is presented in Fig. 2a, where the analog signal (trace 4; purple) can be seen.

The AFE signal conditioning stage consisted of a high-fidelity low-noise signal amplifier and a filter bank as depicted in Fig. 5a. We employed a 20 dB default amplification with no filtering. Note that the input signal (from the database) is pre-filtered to be within the 0.5 to 150 Hz frequency band at the source. This amplified signal is then passed on to the ADM. Although both the AFE and SNN cores are located within the same die, we have extracted the output events from the ADM sequentially, i.e., channel by channel, (for limited I/O of the AFE on the die as compared to the number of input EEG channels) before sending these simultaneously from off-chip to the SNN cores (Fig. 5b).

5.3 Delta modulated EEG events

Asynchronous Delta Modulation[44,45] is a delta modulation approach where the sampling interval is adapted based on the characteristics of the coded signal. In the current context, it represents a level shifter circuit that outputs an event based on the difference in the amplitude of a signal between two sampling points. If two sample points (which might not be consecutively placed, representing asynchronous sampling obeying causality) of a signal show

a change in amplitude that is more than a preset delta-threshold, the encoder records an event. An *'UP'* or *'DOWN'* tag is attached based on the polarity of the change, i.e. if the signal has increased or decreased at the level crossing. Further details on the circuit schematics of the AFE and the ADM can be found in Sharifshazileh et al.[29]. Due to the initial stabilization of analog components within the AFE circuit, we obtained 320 second snippets of each channel for a given seizure following a discarded two-minute pre-seizure segment.

5.4 Analog neurons with digital routing

Figure 5b shows the block diagram of DYNAP-SE2 comprising four neuron cores and the AFE. Each core contains 256 Adaptive Exponential Leaky-Integrate-and-Fire (AdEx I&F) neurons, totaling 1024 (Fig. 1e). All neuron parameters, i.e., time-constants of the synaptic compartments and soma, gain, threshold, and refractory period are shared within a single core. In other words, only four sets of parameters can be assigned within the entire chip. Within this work, all parameters except the time-constants of the neuron cores are kept constant. Each neuron has 64 synapses that can receive spikes from any neuron throughout the whole chip and can be connected to up to 1024 post-synaptic neurons. In the event of an incoming spike, up to four synaptic currents are generated, their magnitudes based on 4-bit weights, that are added and fed into one of four synapse types: fast excitatory (AMPA-like), slow excitatory (NMDA-like), slow inhibitory (GABA-B like) (Fig. 5c) and fast inhibitory (GABA-A like) that acts as a shunt to the soma. The latter synapse type is not used in this work. Throughout the chip, there is a 20–30% variation on all parameters as a result of the subthreshold MOSFET design and the 180 nm manufacturing process[38]. Circuit diagrams of the DPI circuits and a description of additional features can be found in Richter et al.[27].

5.5 On-chip SNN parameters

Tables 2 and 3 describe the relationship between the rise and decay times of the neuron membrane potential as a result of a single spike for all neuron types in this work's proposed SNN. A high time constant leads to a lower rise and decay time as the decay of the synaptic current is reduced. This confirms that the FF neurons are more sensitive to low frequency inputs. Similarly, the rise time of the NLNG neuron is the longest: the decay time is not due to fewer connections, as it has the lowest time constant. For each measurement, the number of equivalently weighted synapses, referred to as the "weights" in the SNN, are set to ensure that the membrane potential reaches a value close to the threshold. In the case of the SNN in this work, the number of equivalent connections of the translation layer is set to ten throughout all translation layer synapses and one or two in the NGNL layer. Such heterogeneous neuromorphic processing systems with mixed-signal analog/digital electronic circuits are extremely noisy and imprecise owing to their sub-threshold operation with very small currents. Thus, the values mentioned in the parametric tables are an estimation and more insights into the hardware effects on parametric values can be found in Zendrikov et al.[38].

Neuron type	$\tau_{\mathbf{rise}}$ **(ms)**	$\tau_{\mathbf{decay}}$ **(ms)**	ΔU **(mV)**	**No. of connections**
$U_{\text{mem}}^{E,I}$	46.1	378.7	248.6	5
U_{mem}^{FF}	8.9	153.8	86.2	6
U_{mem}^{NLNG}	74.6	274.3	43.8	4

Table 2. Measured change in voltage, and rise and decay times of the membrane potential as a result of a single excitatory spike input per neuron type.

Neuron type	**R - E exc. / inh.**	**R - I**	**FF**	**NLNG**
$I_{\tau_{\text{exc/inh}}}$ (pA)	44.1 / 356.4	44.1	66.5	17.8
$I_{w_{\text{exc/inh}}}$ (nA)	16.7 / 34.4	16.7	16.7	16.7

Table 3. The bias generator currents on DYNAP-SE2 for setting network weights and synaptic compartment time constants (excitatory (NMDA like) and inhibitory (GABA-B like)).

5.6 Statistical measures

To quantitatively determine the correlated state of NLNG neurons across long time-scales, namely, synchronization, we apply the inner product between kernelized spike trains of neuron pairs and use the Manhattan (L_1) norm of this product.

5.7 Kernelizing spike-trains to continuous functions

Due to the loss of information from spike-train binning, we have transformed spike-trains into continuous functions by means of kernelization[35]. This kernelization is described by a convolution

$$f_i(t) = i * h \tag{4}$$

where i represents the spike train of neuron i as a sum of delta dirac functions and h is the kernel, represented by a causal exponential decay[35,46]. These can be described by

$$i(t) = \sum_m \delta(t - t_m) \tag{5}$$

$$h(t) = \begin{cases} e^{-t/\tau}, & \text{if } t \geq 0 \\ 0, & \text{otherwise} \end{cases} \tag{6}$$

where t_m represents the spike time of spike m and τ is the time constant assigned to the kernel h. Here, τ is set to 1 ms to include the long and short-term effects of spikes. Due to the nature of spike trains, eq. 5 can be rewritten as

$$f_i(t) = \sum_m h(t - t_m) \tag{7}$$

where $f_i(t)$ becomes a continuous exponentially decaying function starting from each spike.

5.8 Manhattan norm and synchronization matrices

The inner product between pairs of continuous spike trains, defined by eq. 7, is described by

$$< f_i, f_j > = \sum_{m,n} \int h(t - t_m^i) h(t - t_m^j) \mathrm{d}t \tag{8}$$

where $< f_i, f_j >$ is the inner product between f_i and f_j representing the continuous forms of the spike trains of neuron i and neuron j respectively, further details in Ref.[47]. Now we take the Manhattan (L_1) norm of this inner product as a measure of synchronization

$$|| < f_i, f_j > ||_1 = \frac{1}{T} \sum_t < f_i, f_j > \tag{9}$$

where $< f_i, f_j > \geq 0$ across all i and j. For brevity, we represent this measure as $N_{i,j} = || < f_i, f_j > ||_1$ throughout the paper.

Patient	Age (y)	SWEC label	No. of electrodes	Seizure durations Sez-1/Sez-2 (s)	Epilepsy type
1	19	ID2	42	96 / 260	TLE
2	27	ID9	56	104 / 118	TLE
3	24	ID1	47	125 / 70	TLE
4	31	ID16	59	81 / 67	TLE
5	32	ID4	62	160 / 127	PLE

Table 4. Patient characteristics. TLE Temporal Lobe Epilepsy, PLE Parietal Lobe Epilepsy.

5.9 SWEC-ETHZ iEEG dataset

The intracranial EEG data used in this study (Table 4) were downloaded from a public epilepsy dataset[31], assembled at the Sleep-Wake-Epilepsy-Center (SWEC) of the University Department of Neurology at the Inselspital Bern and the Integrated Systems Laboratory of the ETH Zurich, available from http://ieeg-swez.ethz.ch/. Detailed information about the acquisition methods and patient metadata is contained in Refs.[48,49]. The iEEG dataset is recorded during pre-surgical evaluation for epilepsy brain surgery. The intracranial EEG was recorded with strip, grid, and depth electrodes. The data was pre-filtered to the 0.5 to 150 Hz frequency band, sampled at 512 Hz, and further preprocessed to remove artifact-corrupted channels. Annotated seizure onsets and offsets were obtained from visual inspection of an EEG board-certified, experienced epileptologist. Each patient has recordings of multiple seizure events consisting of three minutes of pre-seizure segments (system state immediately before the seizure onset), the seizure segment (seizure event ranging from 10 s to 1002 s), and three minutes of post-seizure segment (i.e., system state after seizure event). All the information about the dataset was taken from the dataset website[31] and the associated publications[48,49].

Due to hardware-related constraints described previously in AFE section, we have chosen a subset of the short-term dataset containing five patients, 2 seizures per patient. Furthermore, considering a constraint on the number of simultaneous input spike trains to the SNN on the event-based processors[27], we have selected patient data with less than 64 electrodes.

References

1. Breakspear, M. Dynamic models of large-scale brain activity. *Nat. neuroscience* **20**, 340–352 (2017).
2. Lehnertz, K. *et al.* Synchronization phenomena in human epileptic brain networks. *J. neuroscience methods* **183**, 42–48 (2009).
3. Jirsa, V. *et al.* Personalised virtual brain models in epilepsy. *The Lancet Neurol.* **22**, 443–454 (2023).
4. Samiee, S., Lévesque, M., Avoli, M. & Baillet, S. Phase-amplitude coupling and epileptogenesis in an animal model of mesial temporal lobe epilepsy. *Neurobiol. disease* **114**, 111–119 (2018).
5. WHO. *Epilepsy: a public health imperative* (World Health Organization, 2019).
6. Olusanya, B. O. *et al.* Global Burden of Childhood Epilepsy, Intellectual Disability, and Sensory Impairments. *Pediatrics* **146**, e20192623, DOI: 10.1542/peds.2019-2623 (2020). https://publications.aap.org/pediatrics/article-pdf/146/1/e20192623/1081031/peds_20192623.pdf.
7. Asadi-Pooya, A. A., Brigo, F., Lattanzi, S. & Blumcke, I. Adult epilepsy. *The Lancet* **402**, 412–424 (2023).
8. Rahimiazghadi, M. *et al.* Hardware implementation of deep network accelerators towards healthcare and biomedical applications. *IEEE Transactions on Biomed. Circuits Syst.* **14**, 1138–1159, DOI: 10.1109/TBCAS.2020.3036081 (2020).
9. Siddiqui, M. K., Morales-Menendez, R., Huang, X. & Hussain, N. A review of epileptic seizure detection using machine learning classifiers. *Brain informatics* **7**, 1–18 (2020).
10. Koren, J., Hafner, S., Feigl, M. & Baumgartner, C. Systematic analysis and comparison of commercial seizure-detection software. *Epilepsia* **62**, 426–438 (2021).
11. Tang, J. *et al.* Seizure detection using wearable sensors and machine learning: Setting a benchmark. *Epilepsia* **62**, 1807–1819 (2021).
12. Lainscsek, C., Rungratsameetaweemana, N., Cash, S. S. & Sejnowski, T. J. Cortical chimera states predict epileptic seizures. *Chaos: An Interdiscip. J. Nonlinear Sci.* **29**, 121106 (2019).
13. Andrzejak, R. G., Rummel, C., Mormann, F. & Schindler, K. All together now: Analogies between chimera state collapses and epileptic seizures. *Sci. reports* **6**, 23000 (2016).
14. Hannon, T., Fernandes, K. M., Wong, V., Nurse, E. S. & Cook, M. J. Over-and underreporting of seizures: How big is the problem? *Epilepsia* DOI: 10.1111/epi.17930 (2024).
15. Zelano, J. *et al.* Report of the ILAE SUDEP task force on national recommendations and practices around the world regarding the use of wearable seizure detection devices: A global survey. *Epilepsia open* **8**, 1271–1278 (2023).
16. DiLorenzo, D. J. Neurovista: Concept to first-in-man: The war story behind launching a venture to treat epilepsy. *Surg. Neurol. Int.* **10** (2019).

17. Razavi, B. *et al.* Real-world experience with direct brain-responsive neurostimulation for focal onset seizures. *Epilepsia* **61**, 1749–1757 (2020).

18. Mead, C. How we created neuromorphic engineering. *Nat. Electron.* **3**, 434–435, DOI: 10.1038/s41928-020-0448-2 (2020).

19. Chicca, E., Stefanini, F., Bartolozzi, C. & Indiveri, G. Neuromorphic electronic circuits for building autonomous cognitive systems. *Proc. IEEE* **102**, 1367–1388, DOI: 10.1109/JPROC.2014.2313954 (2014).

20. Donati, E. & Indiveri, G. Neuromorphic bioelectronic medicine for nervous system interfaces: from neural computational primitives to medical applications. *Prog. Biomed. Eng.* **5**, 013002, DOI: 10.1088/2516-1091/acb51c (2023).

21. Christensen, D. V. *et al.* 2022 roadmap on neuromorphic computing and engineering. *Neuromorphic Comput. Eng.* DOI: 10.1088/2634-4386/ac4a83 (2022).

22. Indiveri, G. & Sandamirskaya, Y. The importance of space and time for signal processing in neuromorphic agents. *IEEE Signal Process. Mag.* **36**, 16–28, DOI: 10.1109/MSP.2019.2928376 (2019).

23. Mayr, C., Hoeppner, S. & Furber, S. Spinnaker 2: A 10 million core processor system for brain simulation and machine learning. *arXiv preprint arXiv:1911.02385* (2019).

24. Davies, M. *et al.* Loihi: A neuromorphic manycore processor with on-chip learning. *IEEE Micro* **38**, 82–99, DOI: 10.1109/MM.2018.112130359 (2018).

25. Pehle, C. *et al.* The BrainScaleS-2 accelerated neuromorphic system with hybrid plasticity. *Front. Neurosci.* **16**, DOI: 10.3389/fnins.2022.795876 (2022).

26. Moradi, S., Qiao, N., Stefanini, F. & Indiveri, G. A scalable multicore architecture with heterogeneous memory structures for dynamic neuromorphic asynchronous processors (DYNAPs). *IEEE Transactions on Biomed. Circuits Syst.* **12**, 106–122, DOI: 10.1109/TBCAS.2017.2759700 (2018).

27. Richter, O. *et al.* DYNAP-SE2: a scalable multi-core dynamic neuromorphic asynchronous spiking neural network processor. *Neuromorphic Comput. Eng.* **4**, 014003, DOI: 10.1088/2634-4386/ad1cd7 (2024).

28. Corradi, F. & Indiveri, G. A neuromorphic event-based neural recording system for smart brain-machine-interfaces. *Biomed. Circuits Syst. IEEE Transactions on* **9**, 699–709, DOI: 10.1109/TBCAS.2015.2479256 (2015).

29. Sharifshazileh, M., Burelo, K., Sarnthein, J. & Indiveri, G. An electronic neuromorphic system for real-time detection of high frequency oscillations (HFOs) in intracranial EEG. *Nat. Commun.* **12**, 1–14, DOI: 10.1038/s41467-021-23342-2 (2021).

30. Costa, F. *et al.* Robust compression and detection of epileptiform patterns in ecog using a real-time spiking neural network hardware framework. *Res. Sq. Prepr.* DOI: 10.21203/rs.3.rs-3591328/v1 (2023).

31. Sleep-Wake-Epilepsy-Center. SWEC-ETHZ iEEG database. Inselspital Bern and ISL, ETH Zurich.

32. Bartels, J. *et al.* Spiking seizure classification dataset, DOI: 10.5281/zenodo.10800794 (2024).

33. Sava, D. E., Rachel & Indiveri, G. Feed-forward and recurrent inhibition for compressing and classifying high dynamic range biosignals in spiking neural network architectures. *arXiv preprint arXiv:2309.16425* (2023).

34. Newman, M. *Networks* (Oxford university press, 2018).

35. Park, I. M., Seth, S., Paiva, A. R., Li, L. & Principe, J. C. Kernel methods on spike train space for neuroscience: a tutorial. *IEEE Signal Process. Mag.* **30**, 149–160 (2013).

36. Akgun, O. C. & Leblebici, Y. Energy efficiency comparison of asynchronous and synchronous circuits operating in the sub-threshold regime. *J. Low Power Electron.* **4**, 320–336 (2008).

37. Merolla, P. A. *et al.* A million spiking-neuron integrated circuit with a scalable communication network and interface. *Science* **345**, 668–673, DOI: 10.1126/science.1254642 (2014).

38. Zendrikov, D., Solinas, S. & Indiveri, G. Brain-inspired methods for achieving robust computation in heterogeneous mixed-signal neuromorphic processing systems. *Neuromorphic Comput. Eng.* **3**, 034002, DOI: 10.1088/2634-4386/ace64c (2023).

39. Frankle, J. & Carbin, M. The lottery ticket hypothesis: Finding sparse, trainable neural networks. In *International Conference on Learning Representations* (2018).

40. Diffenderfer, J. & Kailkhura, B. Multi-prize lottery ticket hypothesis: Finding accurate binary neural networks by pruning a randomly weighted network. In *International Conference on Learning Representations* (2020).

41. Liu, S.-C., Kramer, J., Indiveri, G., Delbruck, T. & Douglas, R. *Analog VLSI:Circuits and Principles* (MIT Press, 2002).

42. Indiveri, G., Stefanini, F. & Chicca, E. Spike-based learning with a generalized integrate and fire silicon neuron. In *International Symposium on Circuits and Systems, (ISCAS)*, 1951–1954, DOI: 10.1109/ISCAS.2010.5536980 (IEEE, Paris, France, 2010).

43. Bartolozzi, C. & Indiveri, G. Synaptic dynamics in analog VLSI. *Neural Comput.* **19**, 2581–2603 (2007).

44. Inose, H., Aoki, T. & Watanabe, K. Asynchronous delta-modulation system. *Electron. Lett.* **3**, 95–96 (1966).

45. Hawkes, T. & Simonpieri, P. Signal coding using asynchronous delta modulation. *IEEE Transactions on Commun.* **22**, 729–731 (1974).

46. van Rossum, M. A novel spike distance. *Neural Comput.* **13**, 751–763 (2001).

47. Park, S. *et al.* Implementation of visual attention system using bottom-up saliency map model. In Springer, B. (ed.) *Lecture notes in computer science, Artificial neural networks and neural information processing - ICANN / ICONIP*, vol. 2714, 678–685 (2003).

48. Burrello, A., Schindler, K., Benini, L. & Rahimi, A. One-shot Learning for iEEG Seizure Detection Using End-to-end Binary Operations: Local Binary Patterns with Hyperdimensional Computing. In *2018 IEEE Biomedical Circuits and Systems Conference (BioCAS)*, 1–4, DOI: 10.1109/BIOCAS.2018.8584751 (IEEE, Cleveland, OH, 2018).

49. Burrello, A., Schindler, K., Benini, L. & Rahimi, A. Hyperdimensional Computing With Local Binary Patterns: One-Shot Learning of Seizure Onset and Identification of Ictogenic Brain Regions Using Short-Time iEEG Recordings. *IEEE Trans. Biomed. Eng.* **67**, 601–613, DOI: 10.1109/TBME.2019.2919137 (2020).

6 Acknowledgements

We thank Alfonso Blanco Fontao and Microelectronics Design Center, D-ITET, ETH Zürich for providing design and assembly support for the DAC board. We are also thankful to Adrian, Maryada, Chenxi, and other members of the NCS group and the INI admin team for providing a conducive research environment that made this work possible.

6.1 Funding

This work was supported by

Japan Science and Technology Agency, Support for Pioneering Researcher initiated by the Next Generation program (JST-SPRING), JPMJSP2106 (for J.B.),

Swiss National Science Foundation for project 200021_182539/1 (for S.G., M.C., and G.I.),

Swiss National Science Foundation for project 204651 (for J.S. and G.I.),

6.2 Author contributions

6.3 Competing interests

The authors declare no competing interests.

6.4 Data availability

The event-based dataset, available at Ref.[32], is constructed from a publicly available dataset available at Ref.[31]. The output spike-trains from the AFE and the NLNG layer along with the DAC-generated values of the analog EEG signals are published in https://doi.org/10.5281/zenodo.10800794.

6.5 Code availability

Data processing and analysis were conducted in Python 3.*x* and the code has been made available at Ref.[32] and published in https://doi.org/10.5281/zenodo.10800794.

Supplementary Materials for

Encoding seizures with partial synchronization: A spiking neural network for biosignal monitoring on a mixed signal neuromorphic processor

Jim Bartels et al.
*Corresponding author. Email: giacomo@ini.uzh.ch

This PDF file includes:

- Figs. S1 to S15

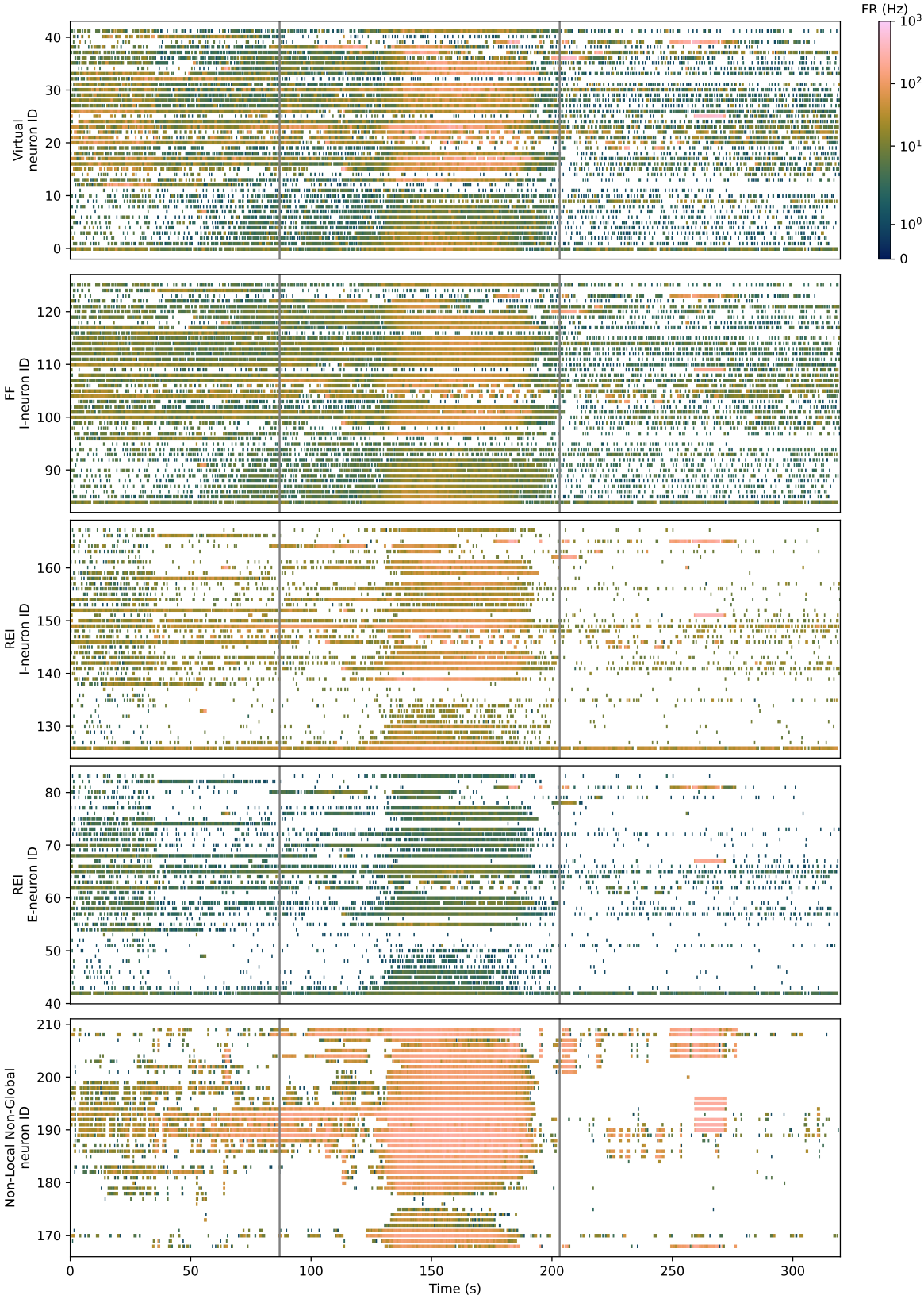

Supplementary Figure S1. Patient 1 seizure 1 output rasterplot from DYNAP-SE2. Grey vertical lines indicate start and end of the ictal period.

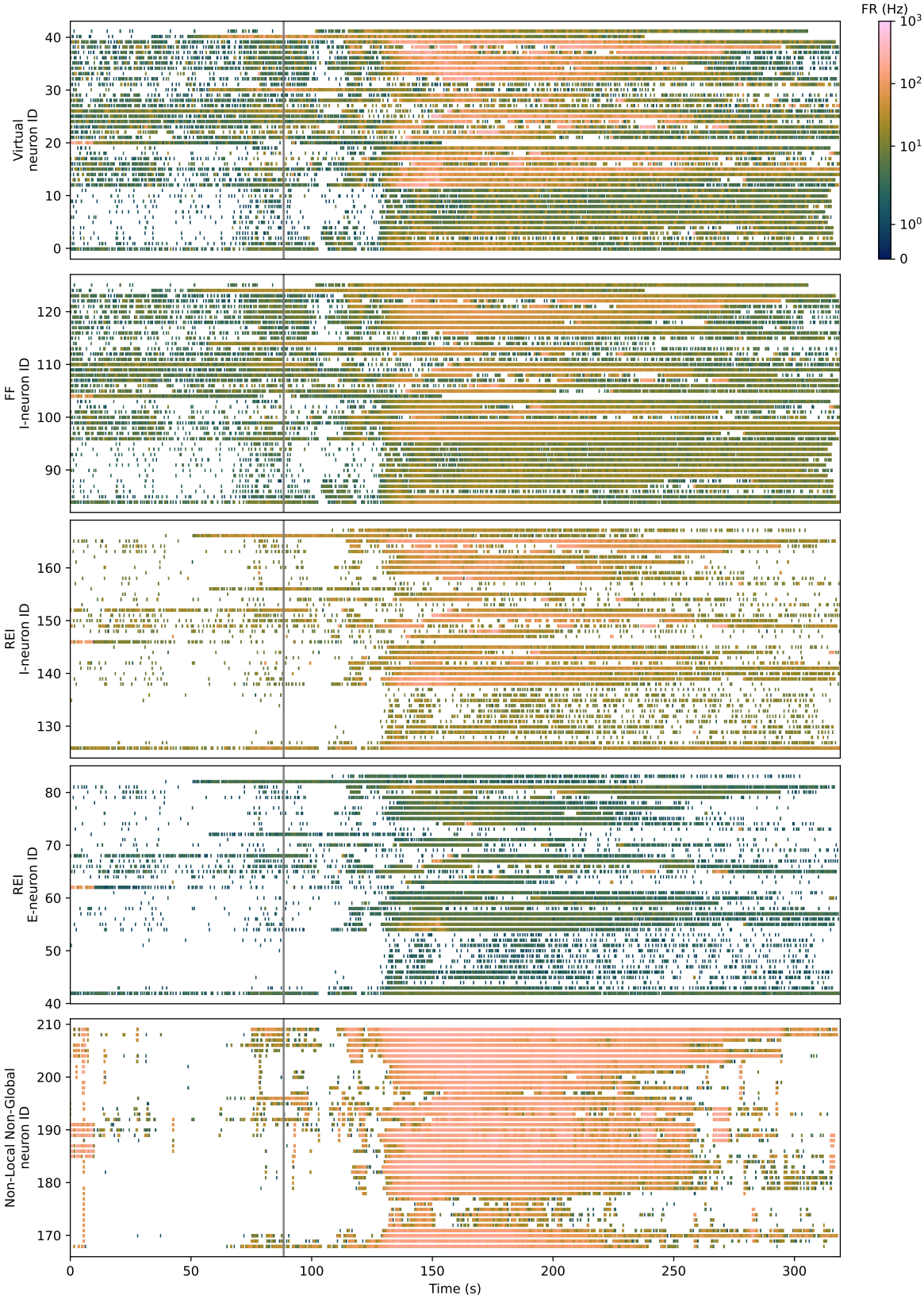

Supplementary Figure S2. Patient 1 seizure 2 output rasterplot from DYNAP-SE2. Grey vertical line indicates start of the ictal period.

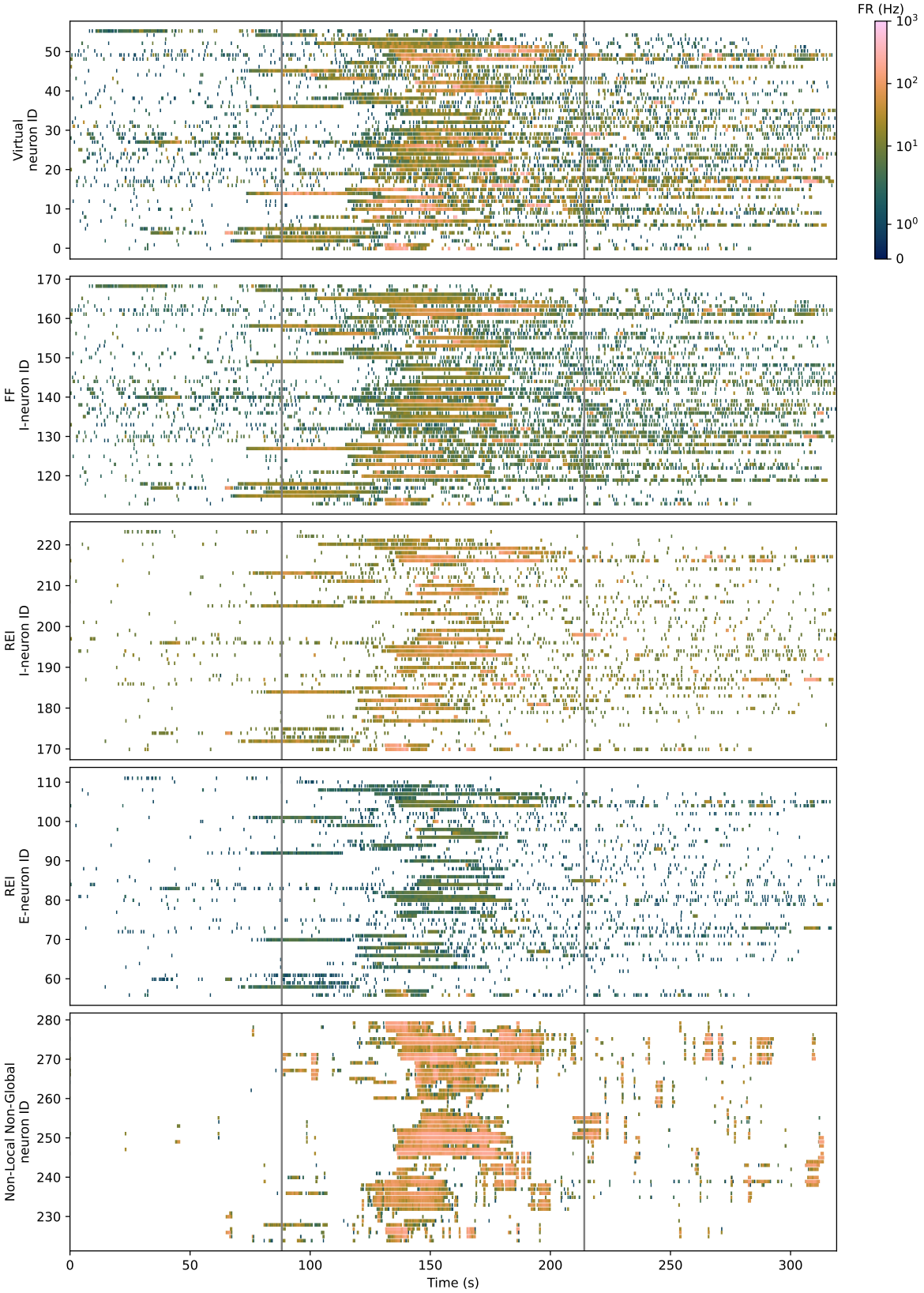

Supplementary Figure S3. Patient 2 seizure 1 output rasterplot from DYNAP-SE2. Grey vertical lines indicate start and end of the ictal period.

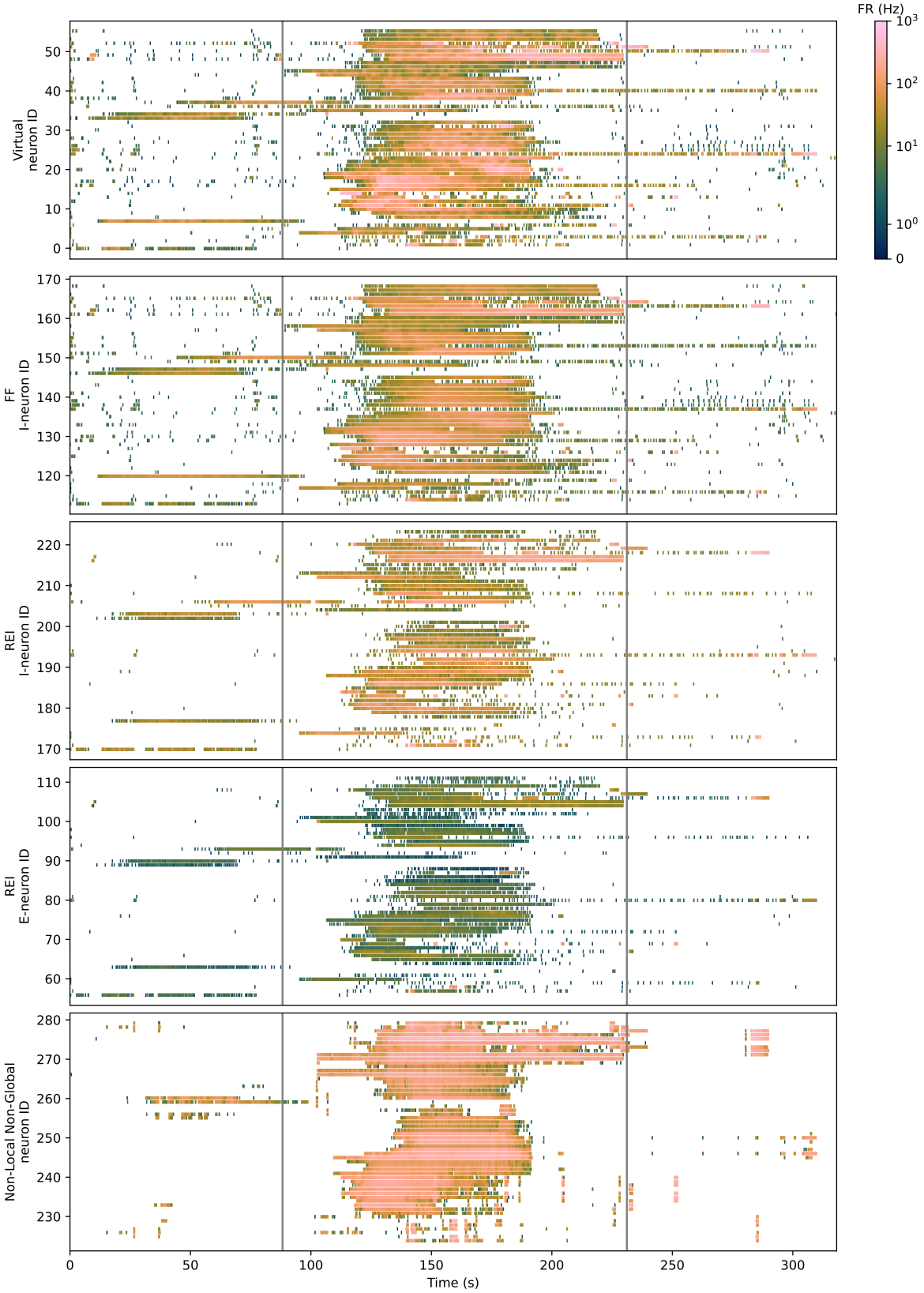

Supplementary Figure S4. Patient 2 seizure 2 output rasterplot from DYNAP-SE2. Grey vertical lines indicate start and end of the ictal period.

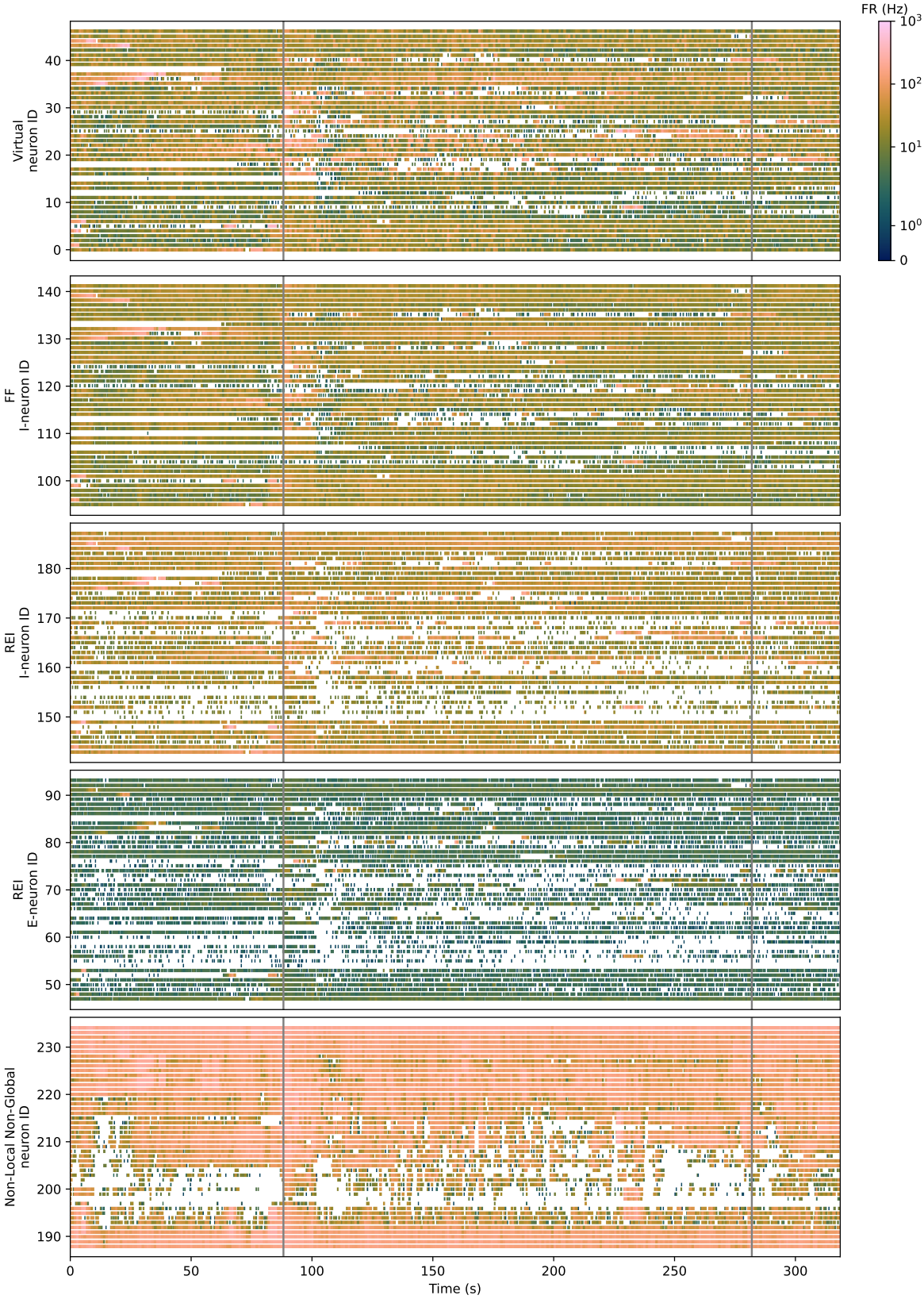

Supplementary Figure S5. Patient 3 seizure 1 output rasterplot from DYNAP-SE2. Grey vertical lines indicate start and end of the ictal period.

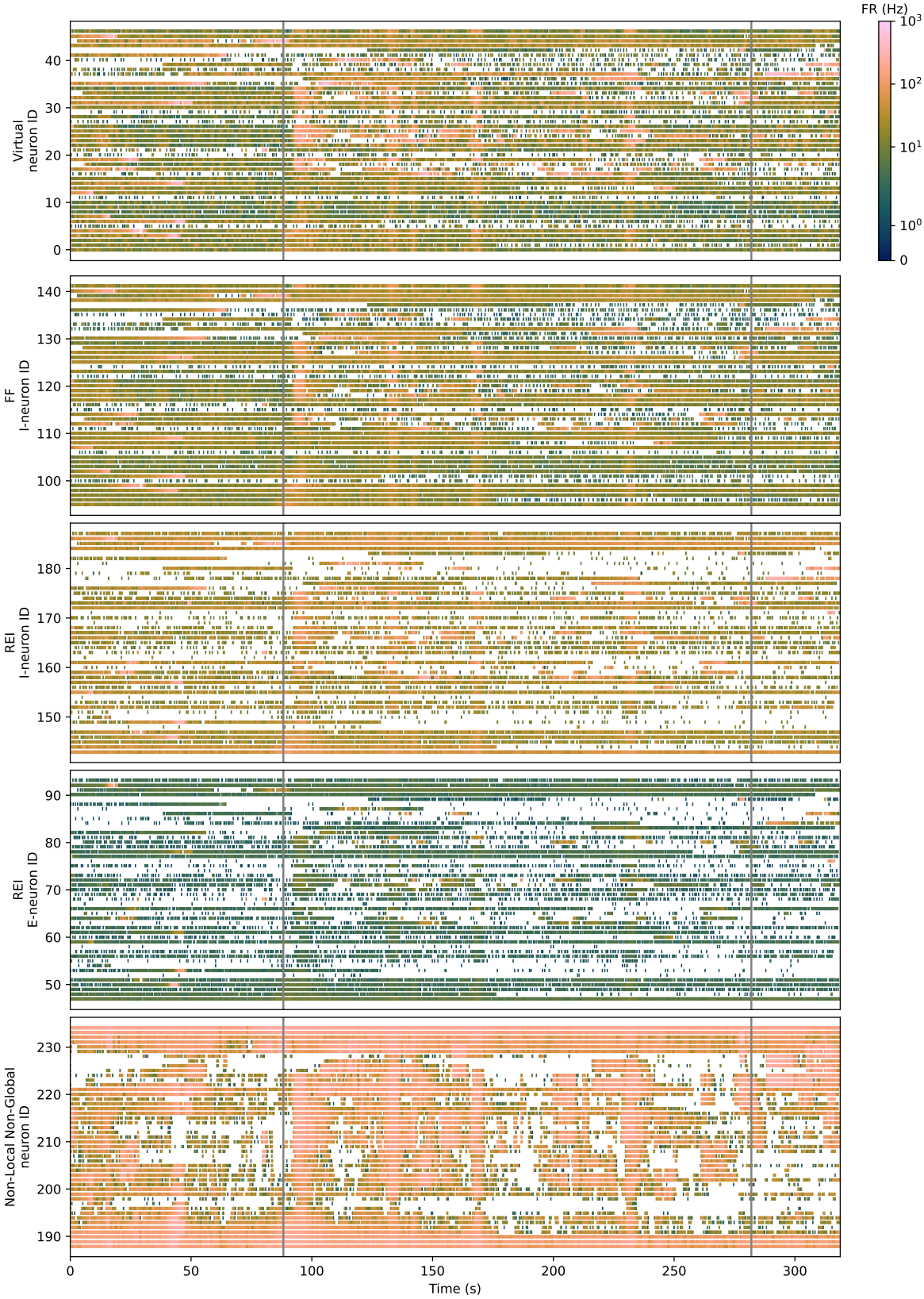

Supplementary Figure S6. Patient 3 seizure 2 output rasterplot from DYNAP-SE2. Grey vertical lines indicate start and end of the ictal period.

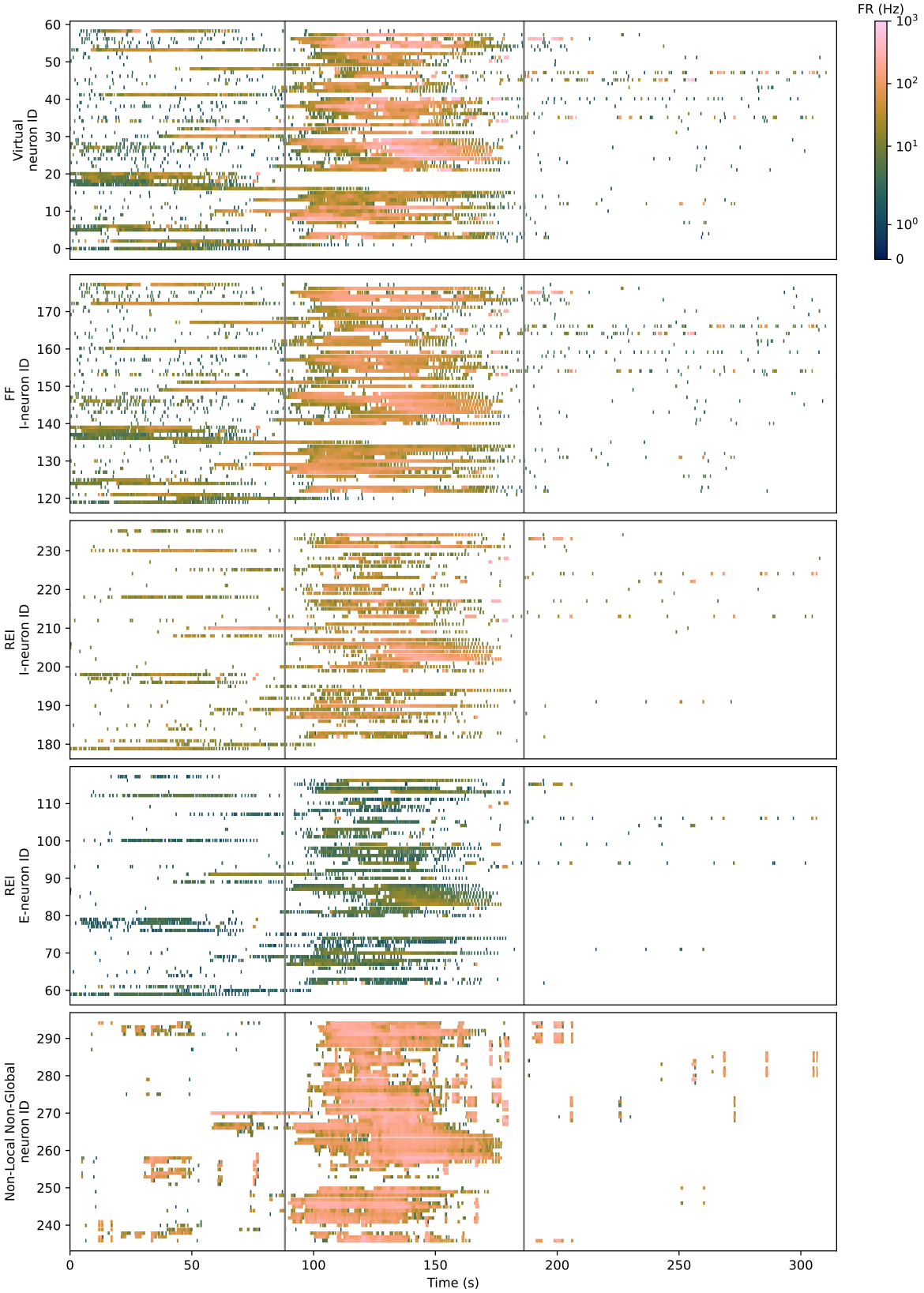

Supplementary Figure S7. Patient 4 seizure 1 output rasterplot from DYNAP-SE2. Grey vertical lines indicate start and end of the ictal period.

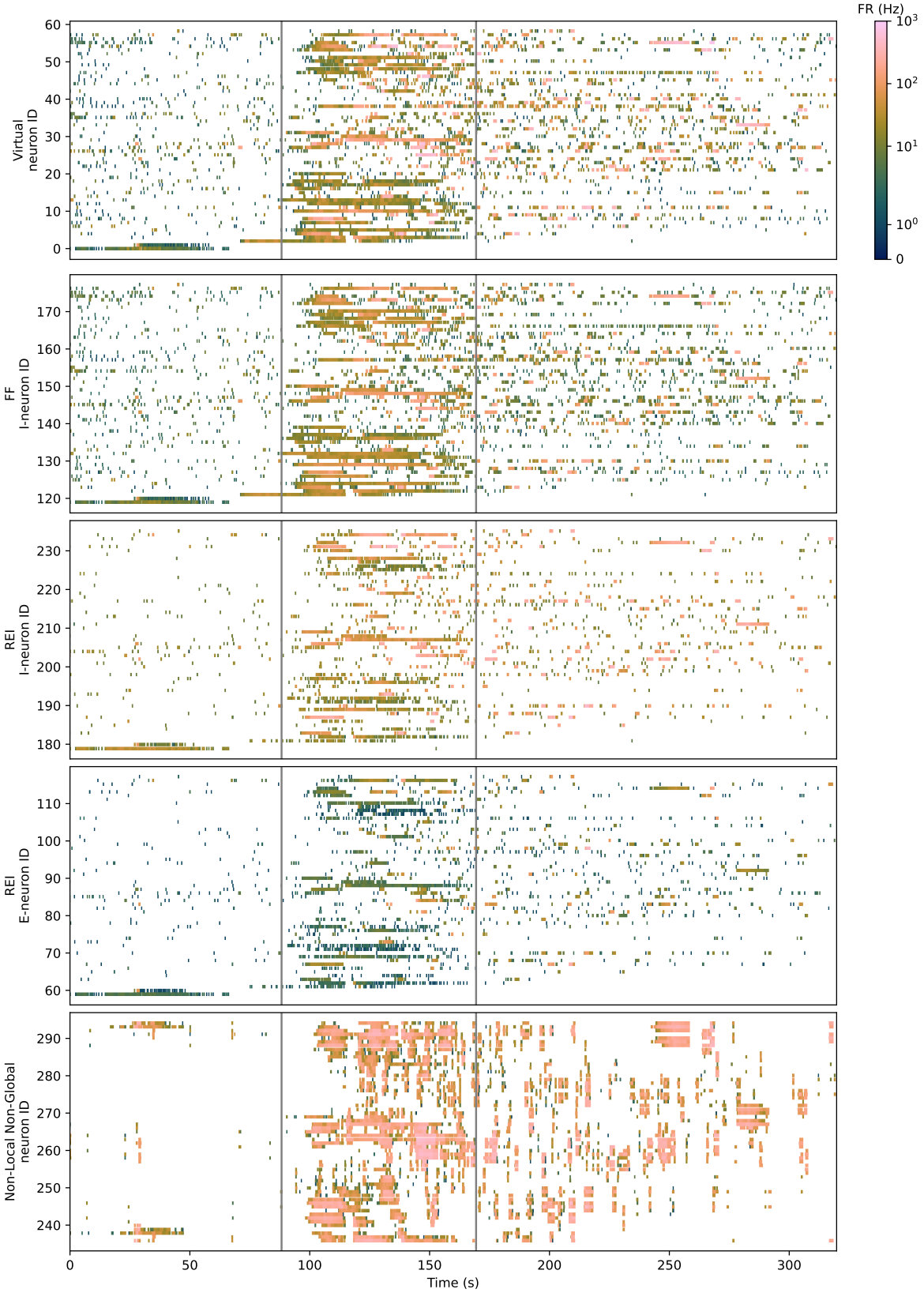

Supplementary Figure S8. Patient 4 seizure 2 output rasterplot from DYNAP-SE2. Grey vertical lines indicate start and end of the ictal period.

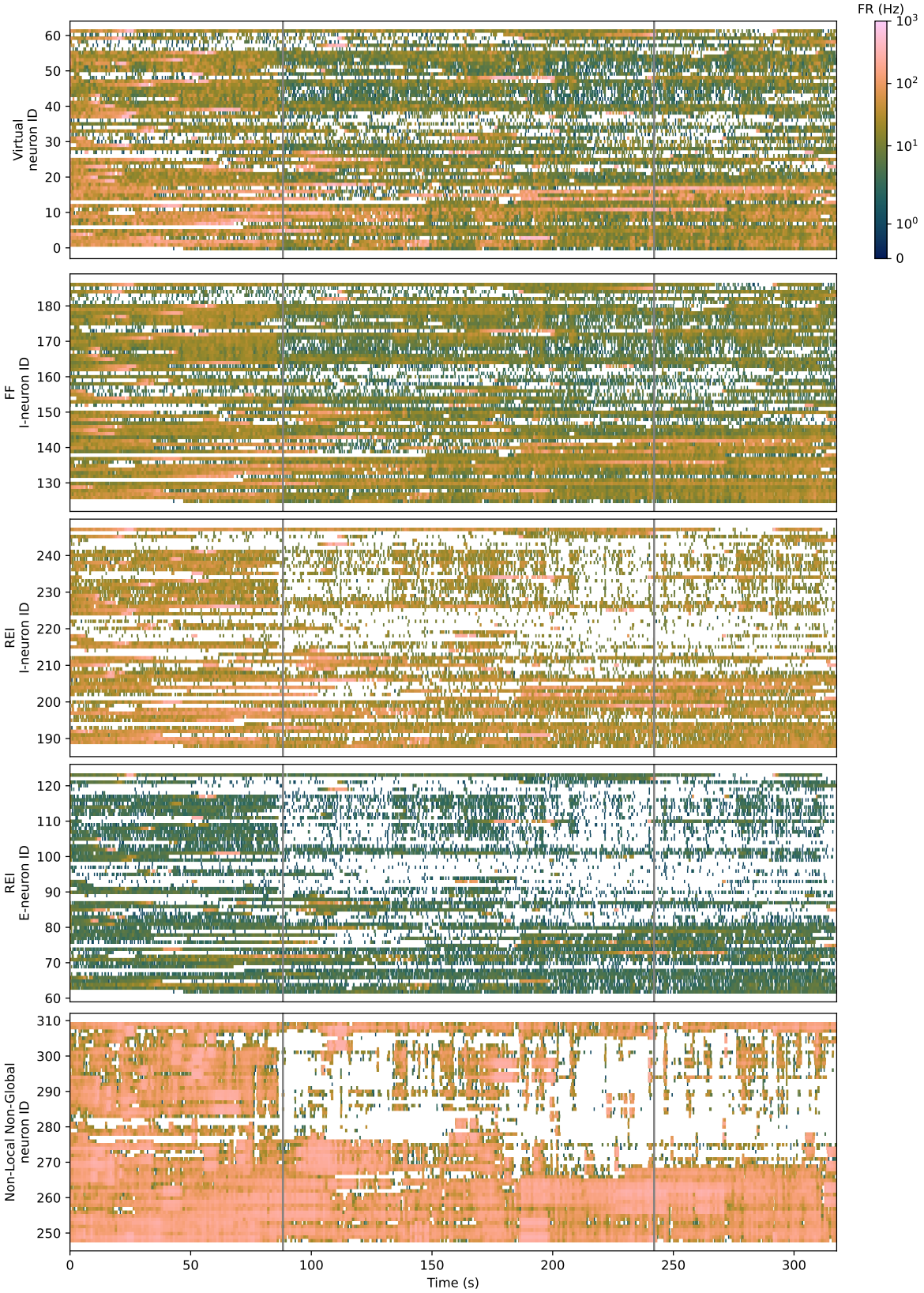

Supplementary Figure S9. Patient 5 seizure 1 output rasterplot from DYNAP-SE2. Grey vertical lines indicate start and end of the ictal period.

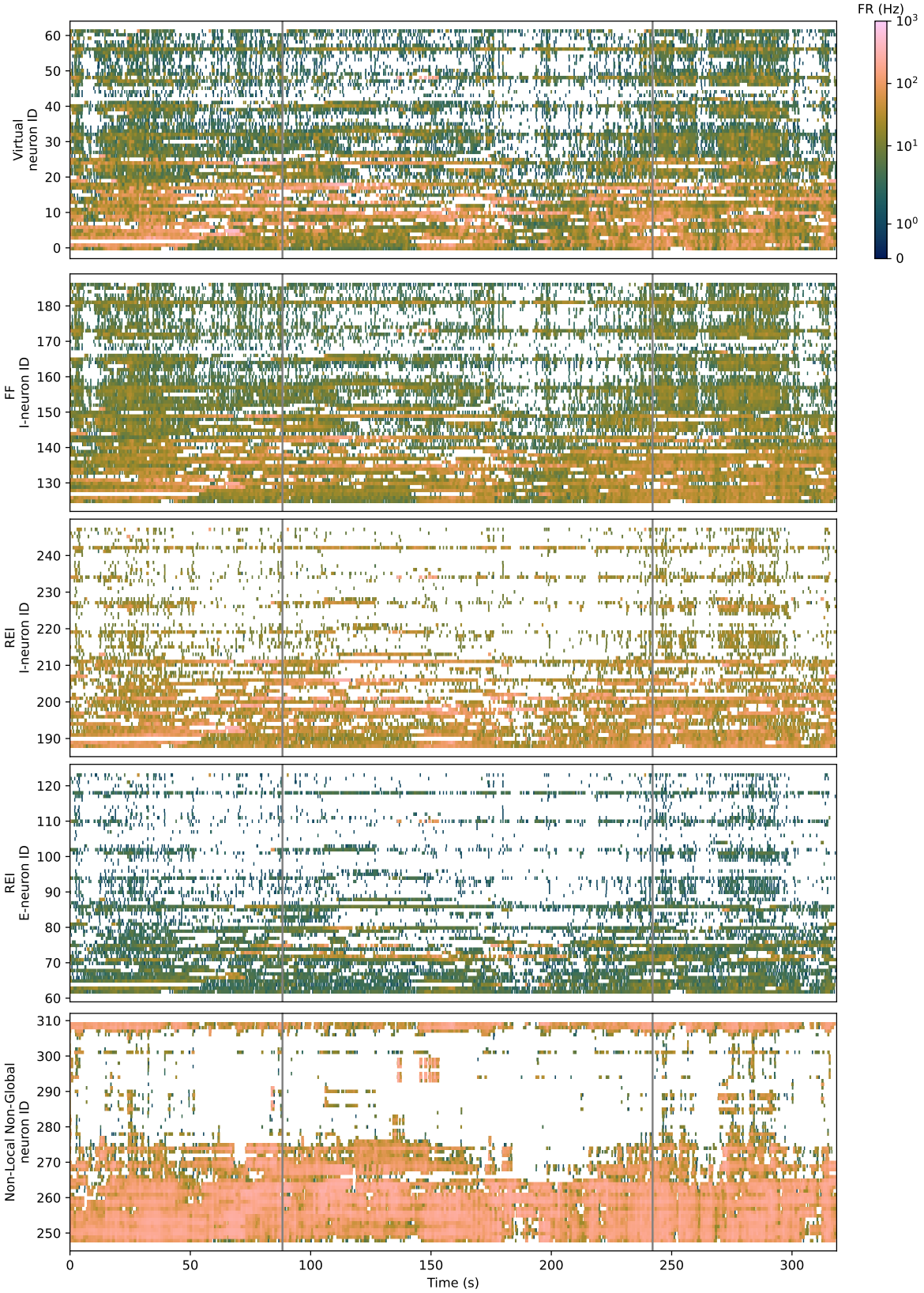

Supplementary Figure S10. Patient 5 seizure 2 output rasterplot from DYNAP-SE2. Grey vertical lines indicate start and end of the ictal period.

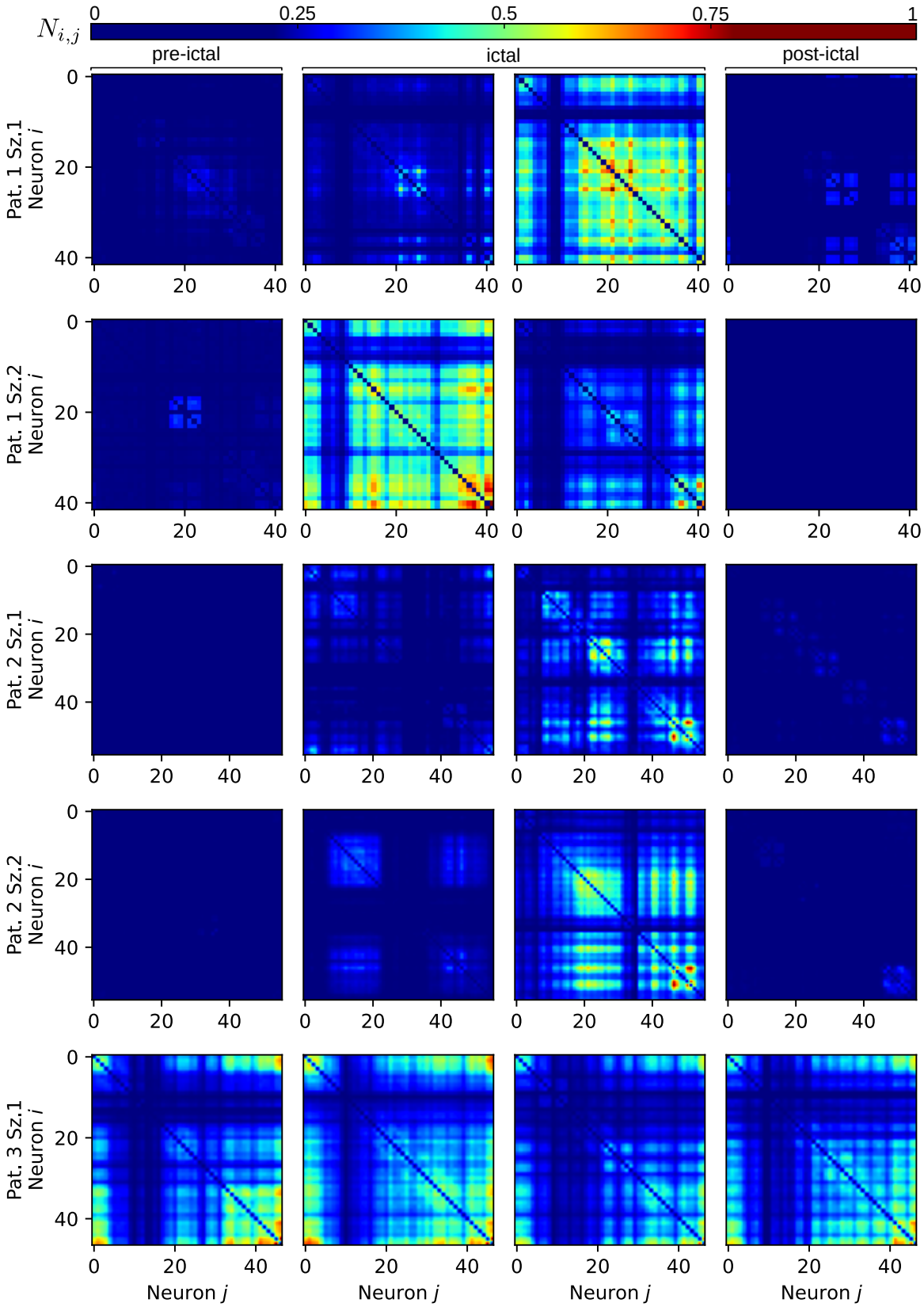

Supplementary Figure S11. Synchronization matrices of Pat. 1, 2 and 3. The columns from left to right show synchronization during the pre-ictal, ictal and post-ictal periods respectively.

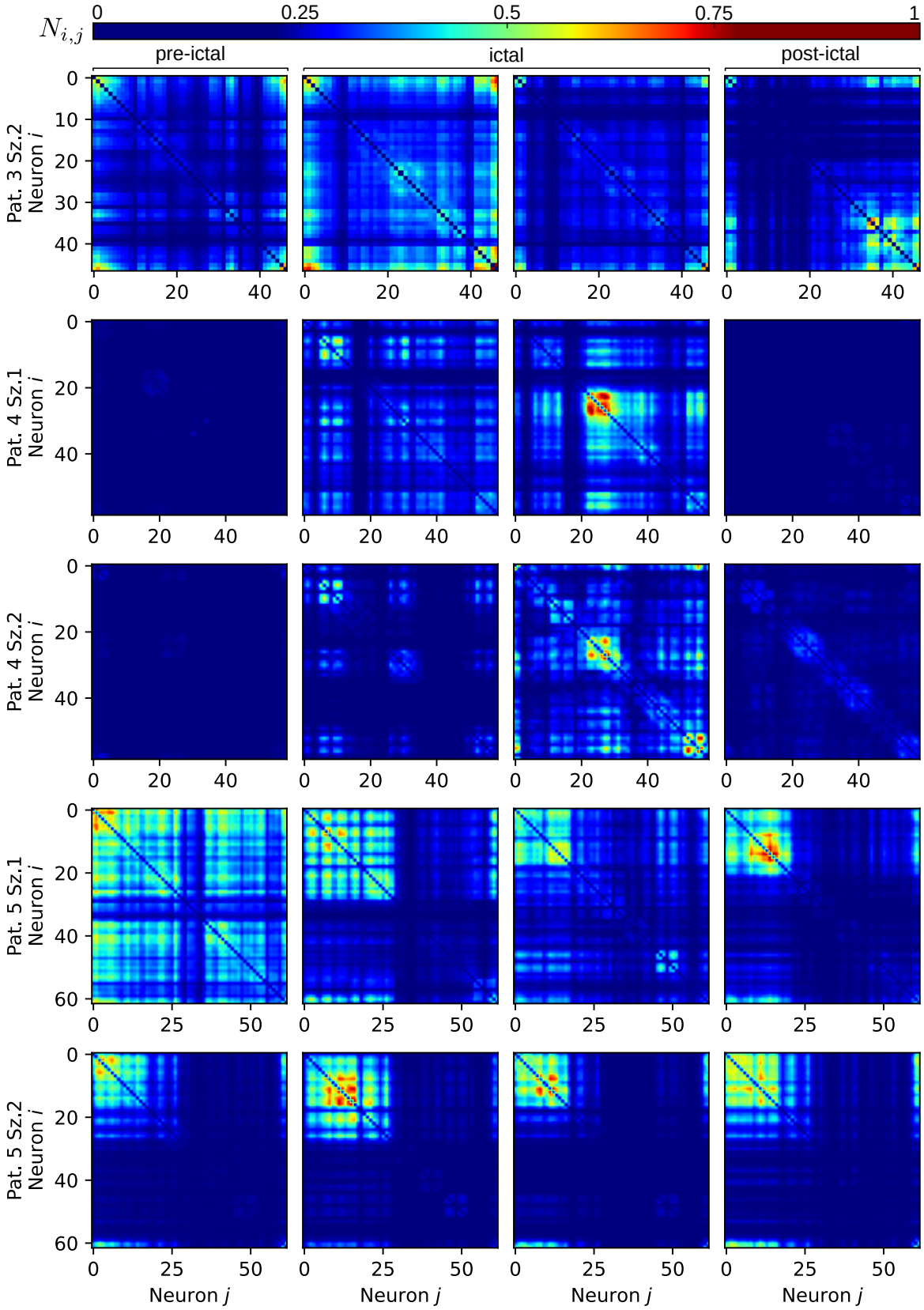

Supplementary Figure S12. Synchronization matrices of of Pat. 3, 4 and 5. The columns from left to right show synchronization during the pre-ictal, ictal and post-ictal periods respectively.

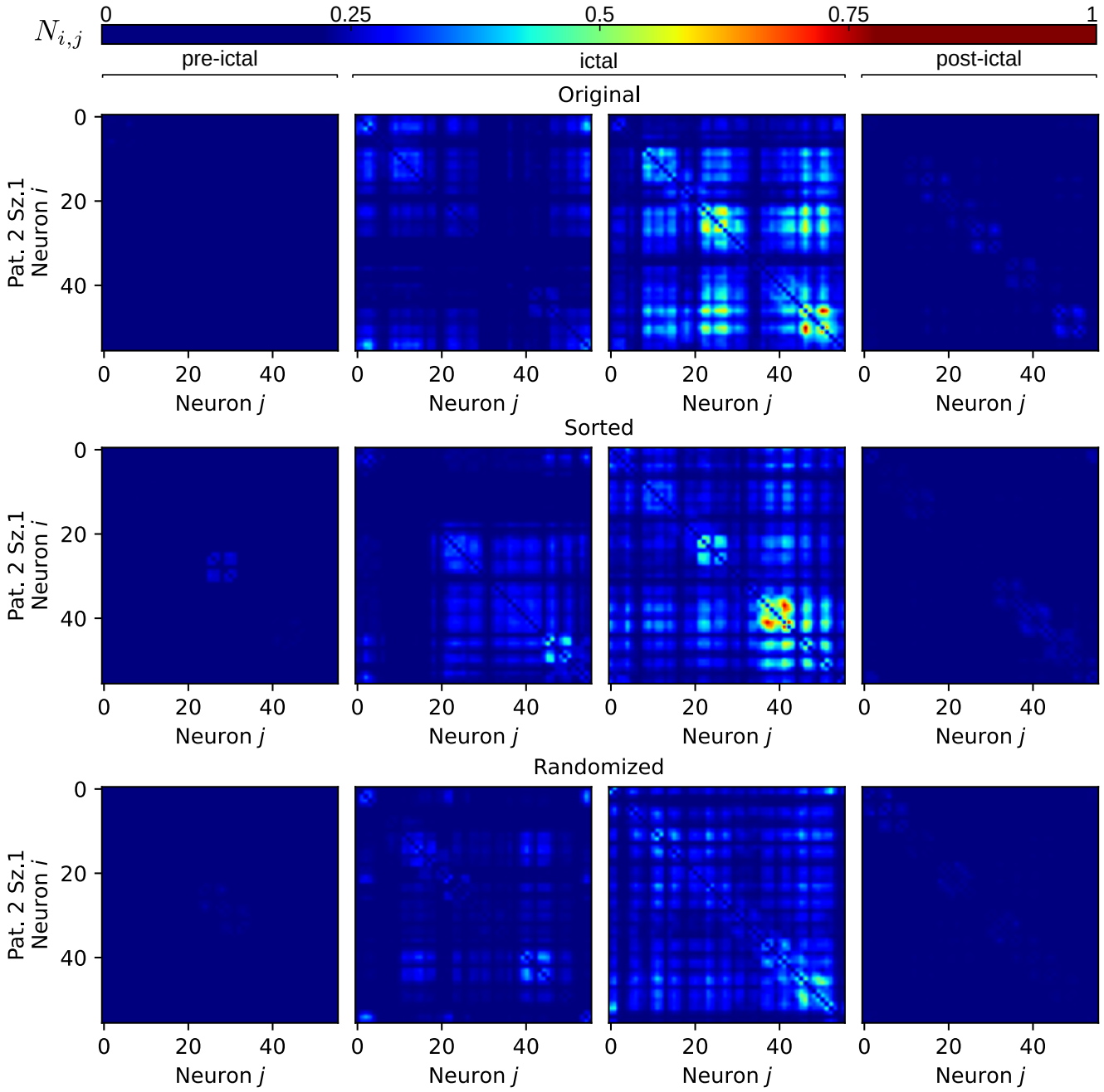

Supplementary Figure S13. Non-local non-global neuron spike train synchronization matrices of patient 2 seizure 1 based on three distinct input channel ordering methods. The first, second, and third rows represent synchronization based on input with the original dataset order, maximum correlation of the original data, and randomized order respectively.

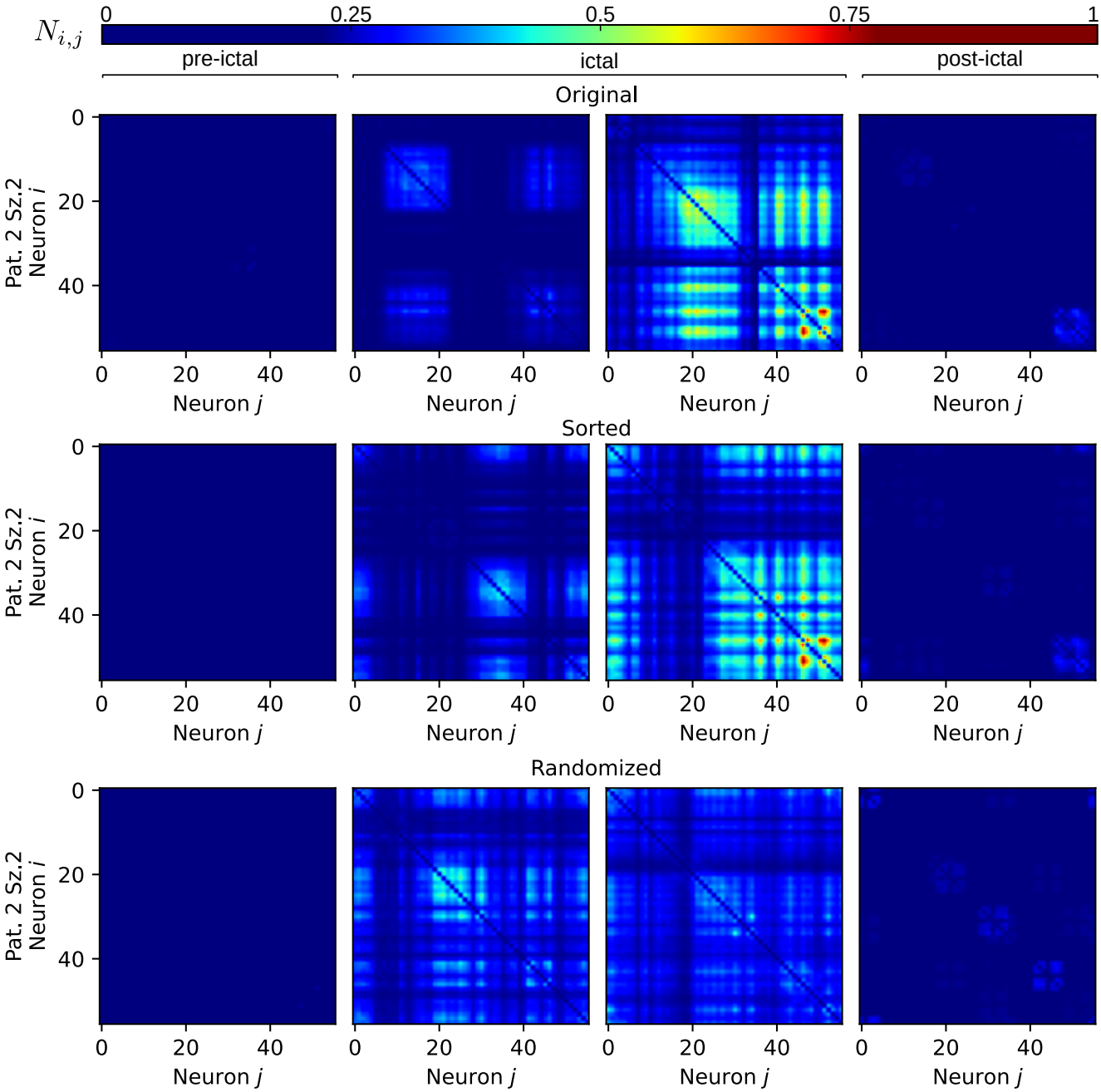

Supplementary Figure S14. Non-local non-global neuron spike train synchronization matrices of patient 2 seizure 2 based on three distinct input channel ordering methods. The first, second, and third rows represent synchronization based on input with the original dataset order, maximum correlation of the original data and randomized order respectively.

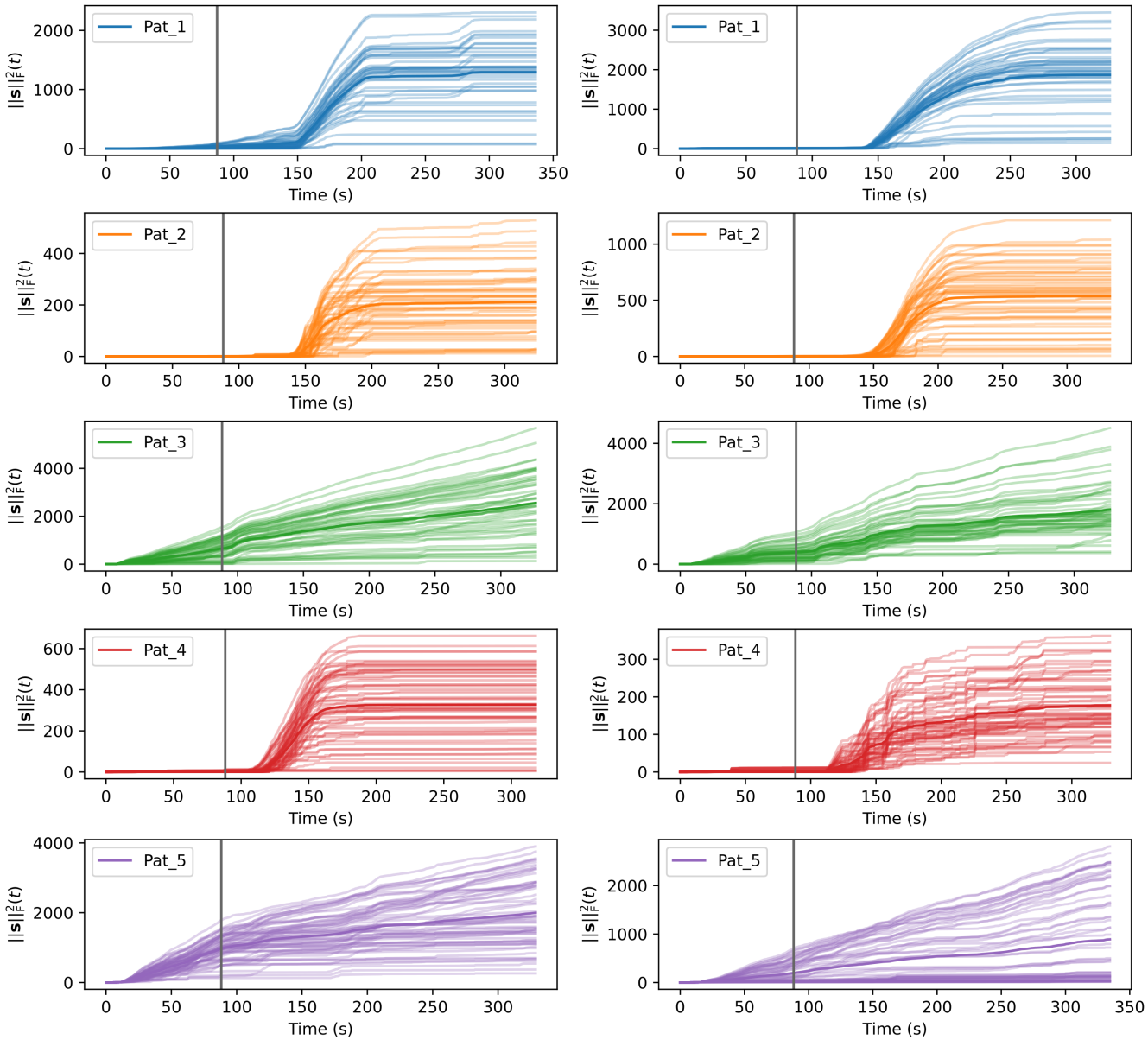

Supplementary Figure S15. The synchronization across all non-local non-global layer neurons over time for all patients and seizures. Grey line indicates seizure start.